

From the Infinitely Large to the Infinitely Small: Applications of Medial Symmetry Representations of Shape

Frederic F. Leymarie¹ and Benjamin B. Kimia²

1: University of London, Goldsmiths College, London, UK

2: Brown University, Div. of Engineering, Providence, USA

V.1 — November 2005*

Abstract

In this chapter we will cover a wide spectrum of applications of medial symmetries of shape from the infinitely large toward the infinitely small. Our journey starts with a dynamic model of the formation and evolution of galaxies. We then move on to the description of geographical information at the scale of regions of planet Earth. Next is the representation of cities, buildings, and archaeological artefacts, followed by the perception of gardens, and the generation of virtual plants. Having reached the scale of human activities, we consider the perception and generation of artistic creations, the study of motion and the generation of animated virtual objects, and the representation of geometrically complex systems in machining, metal forging, object design. We then move inside the human body itself with applications in medical imaging and biology, followed by the representation of molecular structures. Our final stop is to consider the abstract scale of the perception of visual information.

Keywords: Medial axis representations, Voronoi diagrams, galaxy clusters, topography, cartography, cartograms, wireless sensor networks, 3D Geographical Information Systems, architectural axial systems, stylistic signature,

*To be published as Chapter 11, in “Medial Representations: Mathematics, Algorithms and Applications,” Publisher: Kluwer. Editors/Authors: Kaleem Siddiqi and Stephen M. Pizer. Date (approx): Spring 2006.

structural skeleton, biomimetic sculpting, motion planning, animation, shape modelers, shape registration and matching, cell tracking, virtual endoscopy, brain morphometry, growth in embryology, molecular design, contrast sensitivity maps, visual fragments.

1 Introduction

“Do not disturb my circles.” — Archimedes of Syracuse (287–212 BC), last words.

In this chapter we take on a journey covering a full gamut of applications of medial representations of shape, from the large scale features of galaxy formation to the minute description of matter at the molecular level and the abstract scale of thoughts and cognitive processes.

We consider a family of medial representations closely related to and including the medial axes of Blum (\mathcal{MA}) [21]: the Voronoi diagrams (\mathcal{VD}) [123], intensity symmetry axes (IAS) [52], the watersheds of mathematical morphology [152, Ch.9], the (full) symmetry sets [26], the shock graphs [150, 144] and medial scaffolds [101], process inferring symmetries (PISA) [106], generalized cylinders and axes [120], the molecular graphs [10] and critical nets [76].

2 Formation and Description of Galaxies

Consider an extremely large universe, possibly infinite in size, filled with an initially homogeneously distributed gaseous medium. As soon as “perturbations” occur in the distribution, the gaseous mass begins to evolve under its own gravity pulls. The morphological pattern toward which this universe will tend to stabilize itself takes the form of a set of highly dense nodes connected by filaments and walls of lesser density, which mimics the \mathcal{MA} of the original voids, *i.e.*, of the regions of space initially more empty of galactical matter; these voids can be considered as the “generators” of the final morphology.

When the infinite gaseous medium collapses under its own gravity, the regions that happen to be denser than average contract faster, while regions that are less dense than average expand somewhat faster than the rest of the universe. Thus, matter flows away from the low-density regions and towards the zones of higher density. A consequence of this observation is that the low-density regions become

more and more spherical as they occupy more and more volume [45, 71, 183, 72, 182].

In this model of the formation and evolution of the universe on astronomical scales, it is as if matter flows away from the generators (voids) and gathers along *walls*, *i.e.*, the symmetry sheets for pairs of generators. If matters enter the domain of a new cell passed such a wall, its velocity component perpendicular to the wall gets damped by the gravity of the evolving sheet of matter. In time, matter flows along these walls to eventually reach *filaments* where three walls intersect,¹ and where the density is higher than in the walls. Matter keeps flowing along these filaments to finally end at nodal junctions where four such filaments intersect. These nodes “are to be identified with high-density galaxy clusters in the Universe” [183].² This dynamic formation constitutes what Icke and van de Weygaert call “the skeleton of the cosmic large-scale mass distribution by tracing the locus of points towards which the matter streams out of the voids” [183] (Figure 1).

It is interesting here to notice an analogy with the algorithm of Leymarie and Kimia to compute the medial scaffold, a discrete graph-based representation of the 3D \mathcal{VD} and \mathcal{MA} , where, however, “matter” may flow out of certain Voronoi vertex configurations [101, 105, 102].

An early study of stellar arrangements taking the form of \mathcal{MA} or Voronoi tessellations is to be found in the works of Descartes [42, 123]. By 1633, Descartes considered “cosmic fragmentation” in the solar system, *i.e.*, the spatial distribution and relative influence of matter, using Voronoi-like arrangements of solar system bodies — *i.e.*, the Sun, Earth, Moon, and so on — and their surroundings.

3 Geography: Topography, Cartography, Networks

In *topography* one is interested in characterizing the shape of a surface modeling a geographic area, usually much smaller than the Earth, and such that the Earth curvature plays no significant role.³ Then, the surface can be studied as a

¹These are alike the axial curves of the 3D \mathcal{MA} .

²These are alike Voronoi vertices, or equivalently, junction nodes of the 3D \mathcal{MA} .

³One can always project the surface area of interest to undo the effect the Earth curvature, *e.g.*, approximated with a geoid, *i.e.*, a gravitational equipotential surface determining the average sea level, which takes the form of a slightly irregular ellipsoid.

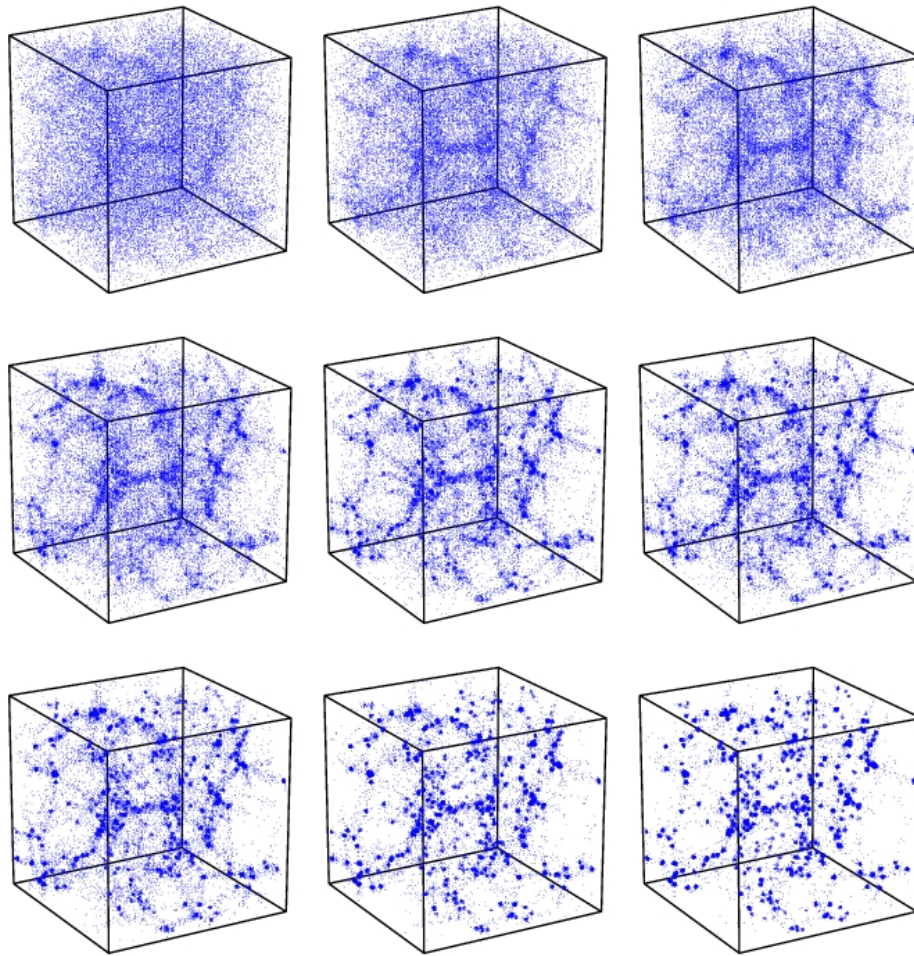


Figure 1: (Adapted from [182, Figure 3], with permission from Rien van de Weygaert.) Example of *galactical systems formation* approaching the 3D \mathcal{MA} of the original voids. Simulation for a cubic volume delineating a cosmic framework for which about 32,000 galaxies have aggregated.

height function of two spatial variables (x, y) .⁴ Typically, one characterizes such a surface via local and regional features. Local features can be, for example, the singularities of the gradient of the height function: minima (pits or sinks), saddles (passes or relays), and maxima (tops or peaks). This classification by peaks, relays and sinks is the classical “hills and dales” representation of Cayley [31] and Maxwell [114] to characterize the topography of a surface by following where water tends to flow if dropped on the surface.⁵ Regional features include the surface lines linking extrema, such as ridges along crest lines, valley lines, and boundaries defined by watershed areas [115].

One way of representing topographical features is to imagine the height function as a 3D object for which we may compute its symmetry sheets such that their extremities correspond to ridges or valleys. Such an analysis can be applied to any height function, not just in the domain of geography, for example, in image analysis.

Gauch and Pizer defined such a \mathcal{MA} for height functions, and called it the *intensity axis of symmetry* (IAS) [52], where intensity refers to their application in the realm of image analysis, where grey level intensity values are taken as heights. In their implementation of this concept, the IAS is made by stacking the 2D \mathcal{MA} of each slice having as boundary a level curve of the image graph, intensity level by intensity level. A level curve in topography is a closed curve such that all its points have the same height. The succession of such 2D \mathcal{MA} when connected along the intensity (height) dimension, creates a set of medial sheets representing a 3D \mathcal{MA} of the image landscape. This is a particular type of “3D” \mathcal{MA} which is oriented along one direction, here the height or intensity dimension.⁶ Gauch and Pizer then extract the ribs of the IAS medial sheets to capture significant ridge and valley lines of the original topography or image landscape.

Another variant of this idea — which can be seen as the opposite to dropping water on a surface — is to construct watersheds by a “flooding” growth simulating a non-necessarily Euclidean propagation from source generators constrained by the surface topography [175, 117]. These “sources” are usually taken as minima

⁴This is the classical Monge patch in differential geometry, *i.e.*, of the type $(x, y, h(x, y))$.

⁵A representation similar to the “hills and dales” of Cayley–Maxwell was advocated by Nackman and Pizer for representing sheets of the 3D \mathcal{MA} itself [118, 119]. For a recent survey and contribution on such concepts, see the work of Koenderink and van Doorn on the structure of relief [82].

⁶The “3D” \mathcal{MA} is obtained as a succession of 2D \mathcal{MA} ’s; this works well here because one deals with a 2D function (of height or intensity). If one directly computes the 3D \mathcal{MA} from the topographical surface, one gets a comparable (but not exactly the same) result.

of the intensity function. The flooding concept is similar to the original “grassfire” idea of Harry Blum [20]: where fronts of “liquid” from different minima first meet, start tracing a “dam” which we can interpret as an \mathcal{MA} sheet in similitude to the IAS method above. The ribs of the final dams when the entire topography is flooded trace ridges; applying the same process on the inverted image traces valley lines.

The IAS and watershed concepts are related in spirit as they target “ridge” and “valley” lines, but they may vary in results, and do vary in construction (of medial sheets). Gauch and Pizer argue for the superiority of the IAS-based subdivision as to which regions are determined [52].

In *cartography*, the 2D \mathcal{MA} has been used to extract and represent roads, rivers and other elongated structures, from aerial or satellite images, to help in the automatic production of maps. From image analysis and semi-automatic initialization, a road might be represented by its centerline, and tracked from a starting point and initial direction [1, 96]. The \mathcal{MA} is also used for other shape analysis purposes, such as the characterization of river banks and area estimates [116]. The \mathcal{MA} is a “natural” and useful representation because it relates opposite points of river banks, relates centerlines or river networks to the “original river bank data,” makes explicit and simple the calculation of surface areas of rivers, and can be used to tie-up the representation of elongated rivers and wider rivers as well as lakes [116].

Gold *et al.* tackle the problem of *map generalization*, *i.e.*, the production of multiscale versions of maps by simplification (of contours, objects, features). They use an iterative process of *retraction* applied to branches of the \mathcal{MA} to simplify it, which in turns smoothes the associated boundaries;⁷ they apply their technique to hydrological networks, elevation contours, and cadastral maps [56]. They also use the \mathcal{MA} to tightly couple level heights of a contour map to regenerate terrain models from these contours, where the \mathcal{MA} is helpful to preserve the topological relation between nearby level heights, leading to valid local terrain slopes [160]. Other applications include watershed and flow estimation from river network input, drainage network estimation from basin boundaries, text recognition and placement in cadastral maps [55].

Cartograms, *i.e.*, geography-related maps deformed to represent statistical information on demographics, epidemiology, agriculture, economics, and so on, can

⁷This is closely related to the more general method developed by Tek and Kimia to structurally smooth 2D contour sets [158, 159]. A 3D analogue of this principle has been explored by Leymarie *et al.* [103].

be constructed and visualized using the \mathcal{MA} [79]. In this application the \mathcal{MA} becomes a local, somewhat deformable and flexible, 2D Cartesian grid where one axis is provided by the \mathcal{MA} itself, and the other is taken as (local) perpendiculars to the \mathcal{MA} . These perpendiculars cut polygonal areas of the map (such as State borderlines of the USA); the cut points are used to stretch or compress parallel-wise to the perpendiculars (or along the \mathcal{MA}) this area of the map (Figure 2). The \mathcal{MA} is particularly useful in this application to keep the deformed map recognizable in shape with respect to the original, untouched, one. That is, the overall topology of the \mathcal{MA} is left unchanged, and the local deformations preserve main features, such as corners or significant curvature extrema of the map, where \mathcal{MA} branches end.

In the area of *wireless sensor networks* an important problem is to plan the routing for static sensor nodes in a geometric space (2D or 3D) with constrained energy supply. The goal is to build a lightweight, efficient structure, constrained by its environment; in particular, geographically close nodes can communicate better. Complex environments, like those in cities, will result in complex shapes of the space where sensors may be deployed, including the presence of “holes,” *i.e.*, due to obstacles like buildings. Connecting a pair of nodes should be done so as to not overload the network, *i.e.*, avoid passing by the same part of the network over and over again.

Bruck, Gao and Jiang apply the 2D \mathcal{MA} to optimize routing in sensor networks [27]. Given a starting and goal nodes to be connected, they use the \mathcal{MA} of the deployment space as a reference to trace a guiding route parallel-wise to the nearest set of \mathcal{MA} branches (Figure 3). Compared to other popular approaches, Bruck *et al.*'s \mathcal{MA} method results in comparable average route lengths, but “much better load balancing.” Modeling via the \mathcal{MA} also leads to good robustness to variations in the network model, a function of the distances between node pairs. Funke reports on a discrete methods to approximate the \mathcal{MA} in sensor networks where nodes have no geometric information. He first evaluates the boundary nodes of the deployment space as well as nodes at the boundary of holes. Then, an approximate distance transform for the deployment space is possible, given the boundary constraints [51]. Bruck *et al.* suggest that, for greater use, their \mathcal{MA} model of routing should be extended to the routing constrained on curved (topographical) surfaces under geodesic metrics, as well as to sensors deployed in 3D space with complex geometries (and with 3D obstacles) [27].

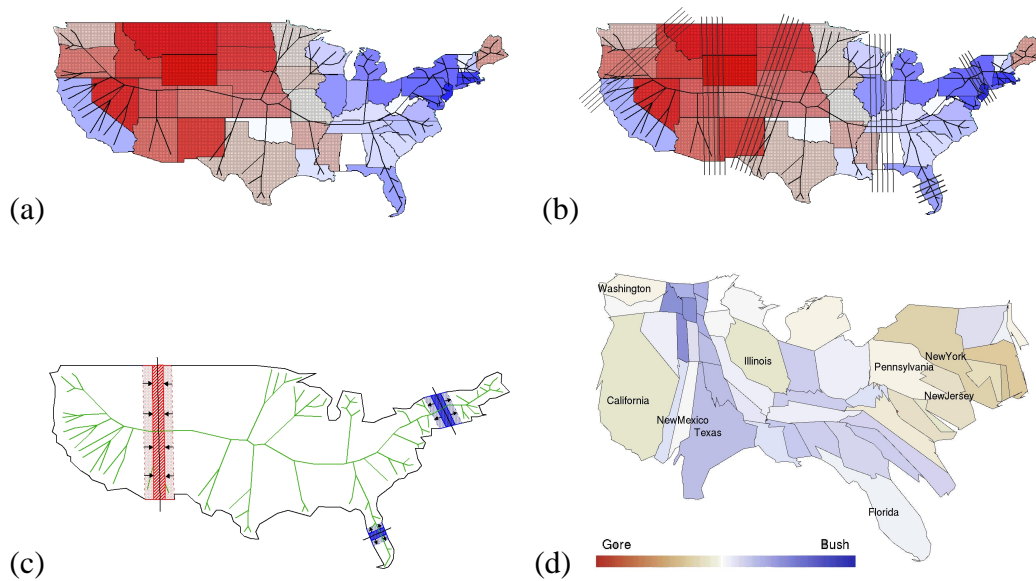


Figure 2: Example of *cartograms* generated using the \mathcal{MA} . (With permission from D. Keim, S. North and C. Panse; Figures 3 and 4 from their “CartoDraw” website [78].) (a) Map of the USA together with the \mathcal{MA} and the population “errors” shown on a bipolar red/blue colormap. Blue corresponds to positive area errors, *i.e.*, blue regions should be larger, red corresponds to negative area errors, *i.e.*, red regions should be smaller, and the darkness indicates the magnitude of the error. (b) Consider an \mathcal{MA} segment (called a scanline) drawn inside a polygon. The algorithm draws line segments (called cutting lines) perpendicular to the scanline at regular intervals [79]. Consider the two edges on the boundary of the polygon intersected by the cutting line on either side of the scanline. These edges divide the polygon boundary into two connected chains. (c) Now, if the area constraints require that the polygon be expanded, the algorithm applies a translation parallel to the scanline to each vertex on the two connected pieces of the boundary (in opposite directions) to stretch the polygon at that point. Similarly, if a contraction is called for, the direction of translation is reversed. (d) State population cartogram for the U.S.A. presidential election result of 2000. The area of each State in the cartogram corresponds to the electoral voters, while the color corresponds to the percentage of the vote. A bipolar colormap depicts which candidate has won each State.

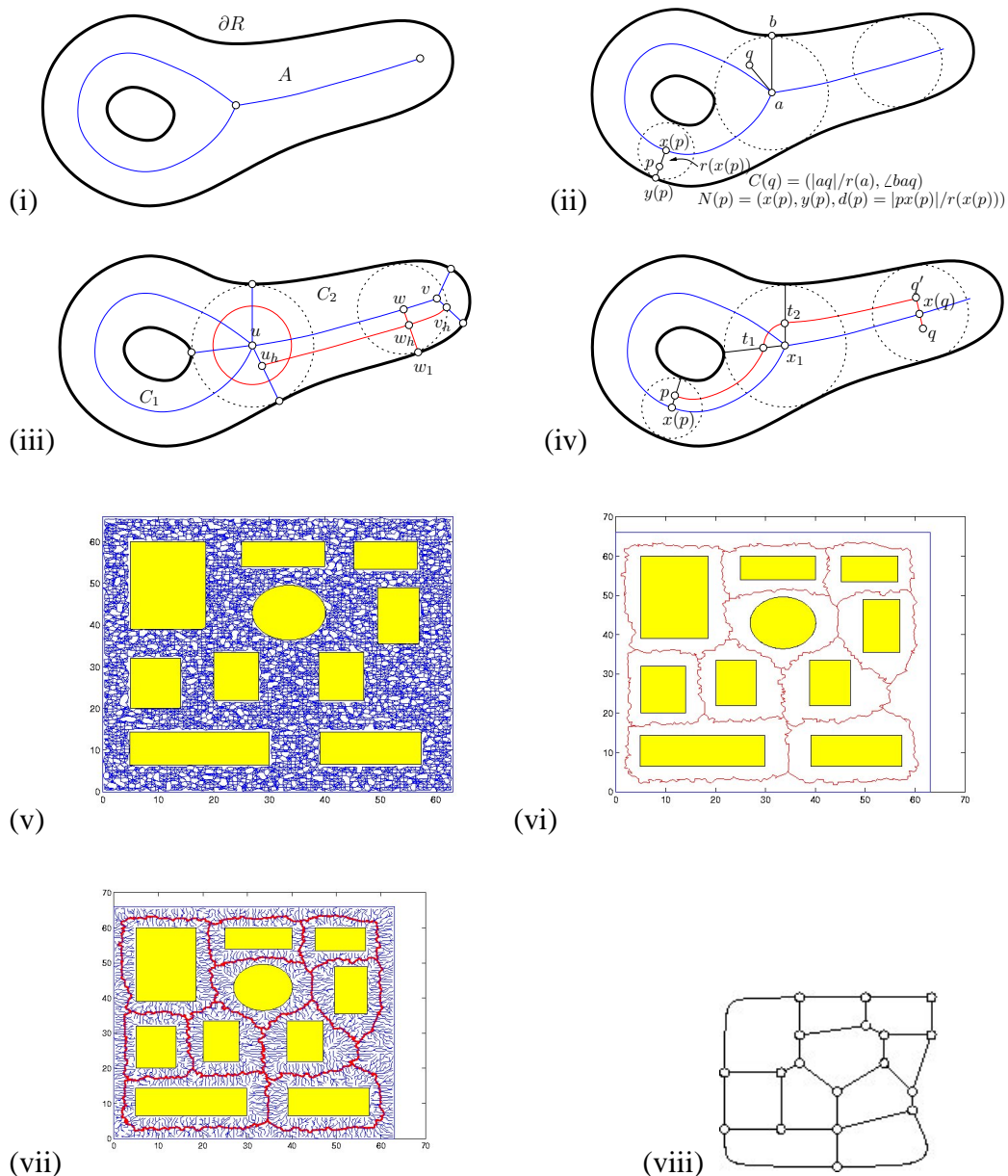


Figure 3: Routing for wireless sensor networks; adapted from [27, (i-iv): Fig. 2, (v-viii): Fig. 9]. (i) An example of the interior \mathcal{MA} of the boundary of a closed region R with two medial vertices. (ii) The naming scheme for a routing protocol based on the \mathcal{MA} . (iii) The road system on R for a routing protocol based on the \mathcal{MA} . Two canonical cells C_1 and C_2 may share a common medial vertex but no common chord. (iv) Routing from p to q . (v-viii) Scenario for a university campus where each sensor has a unit normalized coverage radius. (v) A sensor network of 5735 nodes deployed on a campus, and (vi) its approximate \mathcal{MA} . (vii) The shortest path forest rooted on the \mathcal{MA} . (viii) The \mathcal{MA} graph stored at each sensor.

4 From Urbanism to Architecture and Archaeology

Nearly 50% percent of the world population now lives in cities (closer to 75% in industrialized countries), up from 4% in 1800 and 14% in 1900 [24]. The needs for the 3D modelling of large cities to support efficient *urban information systems* are present and growing, in particular in the domains of urban planning and management, civil protection, environment surveillance and crisis mitigation, and sensor network modelling. One key aspect that requires new technological development is in the management of reconstructed 3D scenery in a geographical context [98]. This in turns calls for a representation of 3D data permitting spatial queries going beyond today's essentially 2D GIS (Geographical Information Systems) [95].

Spatial queries in a 3D graph structure have been proposed by Jiyeong Lee *et al.* to be based on the “straight” \mathcal{MA} , *i.e.*, a simplified medial axis restricted to the description of polygonal layouts [90, 91, 87]. One advantage of abstracting 3D volumes via a medial graph structure is to allow for a hierarchical organization of the data at multiple scales, which is supported by studies on human abstraction of geographic space [30]. In the system of Jiyeong Lee *et al.*, a series of 2D \mathcal{MA} for the communication network (*e.g.*, the hallway structure), augmented to capture all useful horizontal connectivities (*e.g.*, between rooms), are stacked-up and connected vertically to capture the spatial relationships between 3D entities of an entire building. Each augmented 2D \mathcal{MA} represents a level in a building, *i.e.*, typically a floor layout (Figure 4).⁸ This 3D GIS has been augmented to integrate a ground transportation system together with the hierarchical representation of buildings, in the context of emergency responses in times of crisis (such as due to natural disasters, fires, terrorism) [87].

In the context of the built environment, spatial analysis is also fundamental to humans, to create internal images of the urban area, the city, the village. The representation of the built structures is understood as “cognitive maps” which are used to plan movement, and navigate by different means, such as driving, cycling, walking. In particular, predicting human spatial behaviour in urban environments has been modeled by a *space syntax* based on *axial maps* [66, 131]. These maps are constructed from “lines” derived from the main means of communication be-

⁸This use of stratified 2D layouts abstracted by a graph structure, through the \mathcal{MA} , is favored as (i) it naturally captures the important topological structures of human-made buildings, and (ii) it permits to easily extend existing 2D-based GIS systems. Note also, that this construction of a “3D” \mathcal{MA} by stacking-up a sequence of 2D (horizontal) \mathcal{MA} 's is similar to the IAS concept of Gauch and Pizer to model topography (§ 3).

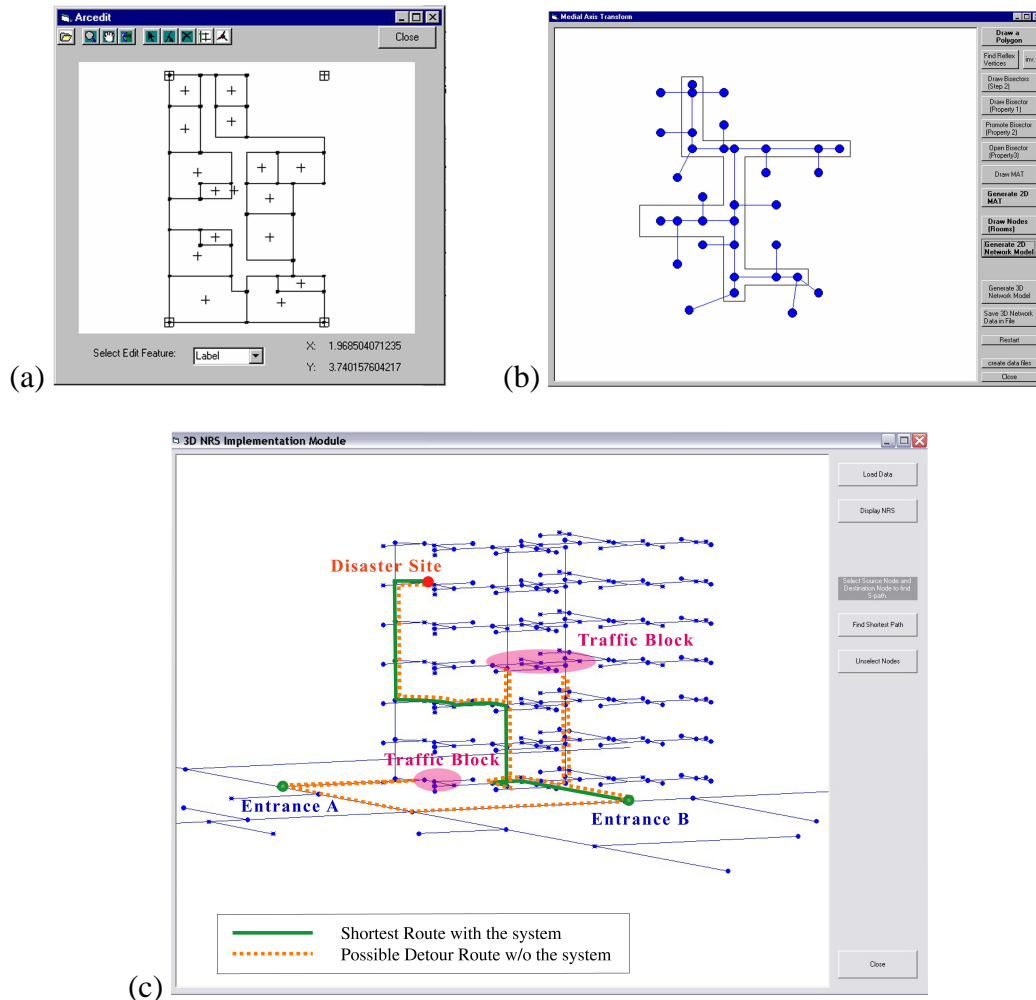


Figure 4: Example of the use of the 2D $\mathcal{M}\mathcal{A}$ to capture form and function in the representation of floorplans, which is then integrated in a GIS model in 3D. (a) The ArcEdit module of the ArcInfo (GIS) software is used as the main interface from which is abstracted (i) a list of nodes representing the rooms (polygons), and (ii) a list of edges representing the communication structure, here a hallway (from [90, Fig. 8]). (b) The straight 2D $\mathcal{M}\mathcal{A}$ generated from the hallway structure in (a) is augmented with links to the nodes representing adjacent rooms, thus capturing the full connectivity structure of a floor (from [90, Fig. 9]). (c) Crisis scenario (from [87, Fig. 10]): Upon arrival at entrance A, the emergency relief crew discovers that it is blocked by debris. Entrance B allows them to enter, but they are blocked by debris again, in the stairway on the 28th floor. Without any knowledge of the communications structure of the building, the crew is likely to go down and up again to find a path to the main disaster area, while with the augmented GIS proposed by Kwan and Lee [87], an optimal path could have been used from the onset.

tween or within buildings, such as roads, alleyways, corridors, and so on. An axial map consists of a minimal set of axial lines which preserves the connectivity of the space, such that every axial line which may connect a pair of otherwise unconnected axes, is included [164]. The concept of an axial line itself comes under various definitions, from the straight centerline of a communication pathway, *i.e.*, its straight \mathcal{MA} , to lines connecting vertices of “obstacles” (*e.g.*, corners of buildings), thus delimiting “isovists,” *i.e.*, the free space that can be seen from a vantage point [14].

An axial map for a given cityscape is then used to measure certain spatial properties such as “connectivity” and “integration” [67]. Connectivity is a local measure computed for a particular axis based on the number of other connected axial branches. Integration is a more global measure which evaluates how many axes need to be traversed to reach a particular goal; this can also be understood as the (topological) depth in the graph one needs to traverse to reach a certain goal from a starting point.

According to Le Corbusier, *architecture* is “based on axes” [38]. Axes are defined by walls, corridors, lighting, the spatial layout of other design elements. “Good architectural design thus enables the observer to extract relevant spatial information” [179]. This is particularly relevant in wayfinding in a building and is known as “architectural legibility” or “intelligibility,” *i.e.*, the capacity of a space to give clues to the understanding of the whole system [66]. The complexity of an axial system for a building can be evaluated in terms of linearity (how straight a path is), connectivity (as for the space syntax above), and consistent alignment with respect to main reference axes (*e.g.*, when moving from floor to floor) [179].

Another major issue in architecture is to capture *form and function* in a uniform, integrated framework. Typically, form is encoded in sets of connected floorplans and profiles delimiting the outlines of main walls, doors, stairways, bathrooms, windows, and so on. Function encodes the integrated relationships of these different elements; that is, not only their respective position and label, but how they interact: *e.g.*, how a door relates one room to another, how a staircase loops around a set of walls. In architecture, “axial systems” capture the “symmetry between objects” [136, 137]. As previously illustrated, applying the 2D \mathcal{MA} to floorplans and profiles offers the possibility to capture the tracing of symmetric outlines — as the envelopes of maximal contact disks centered on the \mathcal{MA} or via sweep functions. Furthermore, it also captures how various elements are interconnected, and how movement through the intermediary created space is possible (Figure 4).

The 3D \mathcal{MA} offers the additional possibility of capturing how volumes are

created both within and outside the architectural structures, specifying their form, volume and topology. The 3D \mathcal{MA} also captures the detailed traces of ridges and associated main central axes of many structural elements used to construct the basic frames of buildings, including walls, floors, ceilings, stairs, ramps, and so on. This is useful for structural analysis as well as for shape rendering in graphics packages based on defining central axes, and sweeping profiles (*i.e.*, the generalized axis representation).

A *generative* theory of shape by Michael Leyton has been applied to architecture, where axes of symmetry (in 2D or 3D) are information carriers summarizing the structure of a building [107, Ch. 15]. One of Leyton's key result is to provide a perceptually and mathematically coherent history for the elaboration of complex architectural spaces.

In *archaeology*, in addition to the above issue of representing form and function in a uniform coherent way, one is faced with the challenge of capturing significant descriptors of shape for the multitude of fragments associated to the original objects [97]. The goal here is one of capturing shape features permitting to, on one hand, posit valid or approximate global alignment positioning, and on the other, extract regional or more local information permitting fine matches between pairs of fragments at their breaks, *i.e.*, along the ridges and corners where they were initially separated by fracture.

One practical approach is to rely on the accurate sampling of the surface of fragments, *e.g.*, via a laser camera system, and compute from such surface representations the 3D \mathcal{MA} for both the inside and outside of each fragment. For example, consider a pot sherd: fragments part of a corner, base, handle, and such, will show distinctive \mathcal{MA} curves (bound to ridges or axial).⁹ In recent studies on systems for the automatic re-assembly of archaeological artefacts from their fragments [165, 93, 37, 127], the main theme is to rely on a fine description of surface breaks or their bounding fracture curves. Here, for example, one can use the 3D \mathcal{MA} for the interior of a fragment to specify the most significant ridges indicative of where the surface initially broke (Figure 5).

Willis *et al.* use a two stage strategy when matching pot sherds. The first stage relies on a probabilistic method to postulate a potential axis of revolution for each fragment, hence specifying the orientation of a sherd [37, 187, 186, 185]. Once an approximate orientation is found for a fragment, other fragments with compatible

⁹The \mathcal{MA} structure for the space surrounding the fragment can be used to find the global positioning of a pot sherd, where its curvature should generate an axial curve aligned with the main axis of revolution of the pot, but this as yet to be used in practice.

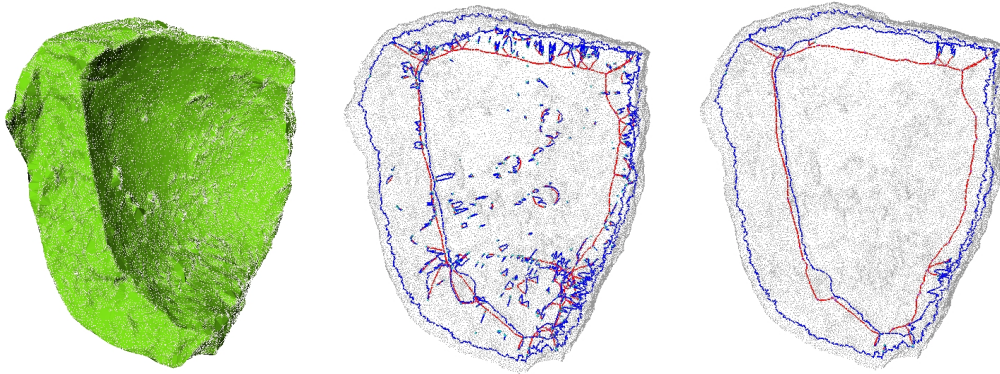


Figure 5: (Adapted from [103].) From the fine detailed laser scanning of a pot sherd (left) to the initial computation of the medial scaffold (graph representation of the 3D \mathcal{MA} , middle), to the simplified scaffold (right) making explicit the most significant surface ridges (blue rib curves of ridges), useful to determine fine matches between pairs of sherds along their breaks. Red curves indicate axial \mathcal{MA} curves, where three (or more) medial sheets meet.

positioning can be looked at for close fine matches in a second stage. Willis *et al.* use a coarse sampling of the most significant ridges indicative of surface break curves to perform close matching of pairs of fragments. Papaioannou *et al.* [128, 127] have developed a general framework for reconstructing 3D objects from their fragments, which is dependent on a good identification of break surfaces and their bounding ridge curves.

In addition to the 3D geometric information these recent systems rely upon, surface and image or color textures, when available across the break curves, should also prove useful to augment the robustness of the matching. Here the 2D \mathcal{MA} can be used in a process of graph alignment or completion for the fine adjustment of matching pairs of sherds. This is particularly useful for those smaller and flatter pieces which show weaker reliable 3D information, for example when the break curves are straight or the interior of break surfaces is very smooth (*i.e.*, without much distinctive local structures).

5 From Garden Layouts to the Genesis of Plants

When contemplating a garden, we often select what we feel are better viewpoints to admire the structure and layout of the landscape, its plants, flowers, rocks, sculptural elements, and so on. Recently, it was shown by van Tonder *et al.* that certain famous 15th century Japanese garden layouts can be modelled by an approximate 2D \mathcal{MA} which represents a perceptual (visual) tension flow field [173, 172, 167, 168].¹⁰

The design of the Ryoanji garden has been a long lasting mystery; van Tonder *et al.* have shown how by using the rock and plant structures of a garden as the generators of a propagation alike Blum's grassfire, an approximate oriented flow field they call the Hybrid Symmetry Transformation (or HST [171]) indicates the best viewing locus.

The dichotomous tree structure of the empty spaces between the five rock clusters of the Ryoanji garden is elucidated by the HST, showing various properties specific to this structure (Figure 6.A2). It clarifies the hierarchical branching pattern, strict branching rule, approximate uniformity of branch nodes, consistent sloping of each branch towards the viewing verandah (bottom of Figures 6.A1 and A2), convergence of the empty space onto the classical viewing location of the garden, and visual balance of the global structure. The branching structure appears to follow the rule of approximate self-similarity of a fractal which is often suggested as a model for vegetation and plants [181, 49]: *e.g.*, it repeats locally in the left most rock cluster of the design (Figure 6.A1).

The approach enables a new level of formal comparison between different Japanese dry rock gardens, and even between Japanese gardens and their counterparts from various locations around the world [172]. Awareness of \mathcal{MA} structure in Japanese gardens motivated new attempts to reconstruct garden maps from old illustrations of Japanese gardens that no longer exist [168]. In this case, \mathcal{MA} analysis brought to the attention at least one lost garden of potential significance (Figure 6.B1), and further helps in the analysis of origin of some gardens, since \mathcal{MA} 's serve to some extent as a *stylistic signature* of the creator of a garden.

While the 2D \mathcal{MA} proves useful to study the "horizontal" structure of a garden, the 3D \mathcal{MA} is often used to help model *plants' architecture*, where the branching structure is built as an assembly of generalized cylinders each representing a branch [44], or more generally via modular graph structures where each

¹⁰Readers familiar with the Japanese language should note that the acronym \mathcal{MA} (medial axis) is not to be mistaken with the Japanese term "ma," denoting the interval between "things," spatial or temporal, although the two *appear* to be related.

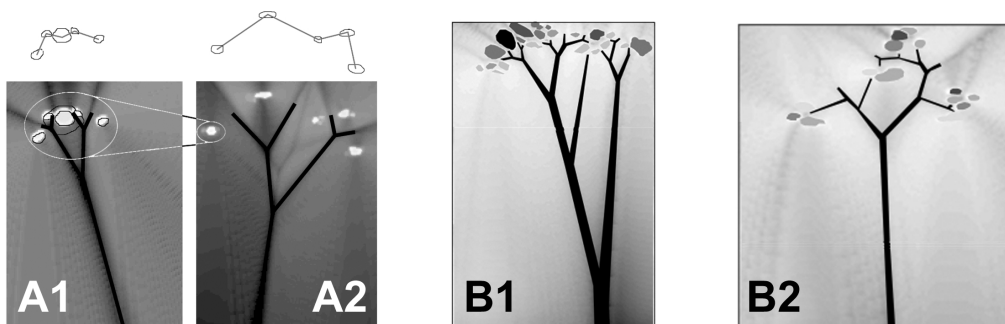
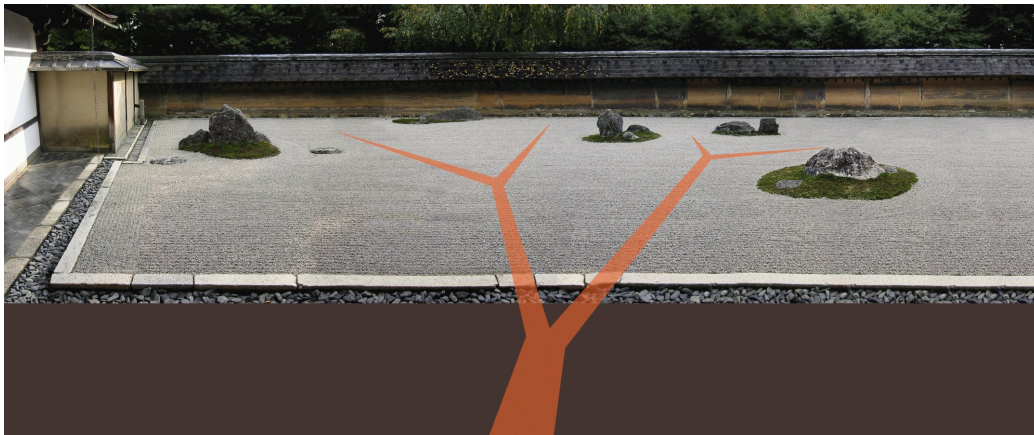


Figure 6: Example of flow field computation specifying the *intrinsic design of old Japanese gardens* (with permission from Gert van Tonder). At the top is shown a side view of the Ryoanji garden (15th century) and below it is shown the same view with the superimposed and projected global \mathcal{MA} . The local and global \mathcal{MA} 's (A1 and A2, respectively) in the Ryoanji temple garden are shown in an “aerial” view on the bottom-left [173]. \mathcal{MA} 's of a reconstruction of the Zakkein temple garden B1, no longer in existence, and a non-realized garden B2, conceived and sketched by Japanese garden connoisseur, Akisato Ritoh (1799). The conceptual garden shares key features with Ryoanji and Zakkein, but lacks the finer aspects seen in the dichotomous trees of the first two examples.

module may represent roots, a set of branches, a single branch, a set of leaves, a leaf and its venation pattern, petals, and so on [140]. Shlyakhter *et al.* use images of actual trees, flowers, and such, to first obtain a 3D volumetric description of the plant by constructing a visual hull from multiple snapshots around it [148]. An \mathcal{MA} is then computed to approximate the main trunk and branches of the original tree.¹¹ Finally, this skeleton is fed to an “L-system” [111, 141] to re-generate a close approximation of the plant which can be used in off-the-shelf graphics renderers; such a process can then be used to populate an entire ecological “context;” for example in applications to forestry, agriculture, horticulture, landscaping.¹² Prusinkiewicz *et al.* use the 2D \mathcal{MA} (in the form of a Voronoi diagram) to control the spacing between “auxin sources” and “vein nodes” to generate biomimetic leaf venation patterns [142].

The above study of van Tonder *et al.* on the use of the 2D \mathcal{MA} to describe and apprehend the spatial layout of a garden is echoed in the works of Richard Toth on developing a theory and language for landscape analysis [162]. Toth proposes that relationships between spatial units can be understood as figure/ground patterns which can be characterised, in particular, via Arnheim’s “structural skeleton” [8].

6 Visual Arts: Painting, Drawing, Sculpting

By the mid 20th century, Rudolph Arnheim had proposed to model the creation and perception of paintings via a tension field whose main force lines constitute what he calls the “structural skeleton” of a painting, drawing, or sketch [8]. This skeleton can be approximated as Blum’s \mathcal{MA} for the exterior of the shapes, within the limits of a canvas, *i.e.*, the lines of symmetries indicating the lines of balance between the canvas (delimiting the outward boundary of the painting or sketch) and the pictorial elements imposed by the creator, the artist (*e.g.*, the lines and outlines of shapes).¹³ Some empirical evidence in support of the ability of humans to detect an induced structural skeleton in paintings has since been reported by

¹¹They call their graph structure a *Voronoi skeleton*, as it is based on algorithms computing the Voronoi diagram of a cloud of points for the vertices of the visual hull.

¹²L-systems (also called Lindenmayer systems or parallel string-rewrite systems) are made from productions rules used to define a tracing of piecewise linear segments with joints parameterized by rotation angles [111, 141]. These rules also are a compact way to iteratively repeat constructive sequences in the description of fractals, often used to model groups of plants, flowers, leaves, and so on [49].

¹³More precisely, Arnheim is thinking of the *full symmetry set* for the space between the canvas and the shape outlines (*e.g.*, see [8, Figure 3, p.13]).

Locher [112]. The use of the \mathcal{MA} as a support for a perceptual tension field can be more generally understood via the Gestalt principles of perception which emphasize features such as continuity and symmetry, in the context of a density field of forces [8, 106, 104] (see also § 11).

This concept has been extended by Leyton, who also represents the inside of painted forms with a 2D \mathcal{MA} where branches are oriented to indicate growth patterns (*e.g.*, of arms and fingers) and exterior pressures [106]. Leyton not only seeks to represent a static view of a painting by describing the exterior and interior balance of the visual field, but further views the directed 2D \mathcal{MA} as an explanation for the shapes drawn on the canvas, *i.e.*, by providing a perceptually plausible dynamic history for the patterns [107, 108].¹⁴

When learning to *draw*, a basic technique to render human forms and gestures is to approximate their skeleton via stick figures, over which “flesh” or structure can be built. Stick figures are also used by infants and primitive cultures in early representations of human or animal forms. A computational system based on generalized cylinders called ROSE (Representation Of Spatial Experience) was developed in the mid-1990’s by Ed Burton to model young children’s drawing [28].

Using a skeletal representation to draw shapes in 2D or 3D has been exploited in some graphics packages. For example, in SKETCH the user can directly draw 3D axes and define sweep functions to “grow” or sweep the outline surface [191], while in “Teddy,” an approximate 2D \mathcal{MA} is used to define the spine of objects sketched in 2D, which are then extruded in 3D to create a final rendering [73]. Related approaches are used in computer graphics to directly generate 3D freeform models using either stacks of 2D \mathcal{MA} (representing sections of objects) [134], full-fledge 3D \mathcal{MA} [166], or curve-like 3D skeletons (alike generalized cylinders; Figure 9) [88, 48, 23, 174, 6]. These models, once equipped with a growth functional (*e.g.*, via a distance or sweep function), can be used to produce 3D figures.

In automatic *painterly rendering*, Gooch *et al.* use the 2D \mathcal{MA} to define brush strokes, *i.e.*, their direction and size. They first segment an image in homogeneous color patches, and then capture the main axial directions of each such patch via an approximate \mathcal{MA} [57]. In automatic *portrait generation*, Tresset and Leymarie use the 2D \mathcal{MA} to define main gesture lines to follow when mimicking the artist’s hand [163]. These “gesture lines” drive the drawing device, *e.g.*, an ink plotter (Figure 7). In automatic *surface shading* to produce illustrations and engravings,

¹⁴This dynamic view of the 2D \mathcal{MA} is called by Leyton the “Process Inferring Symmetry Axis” (or PISA).

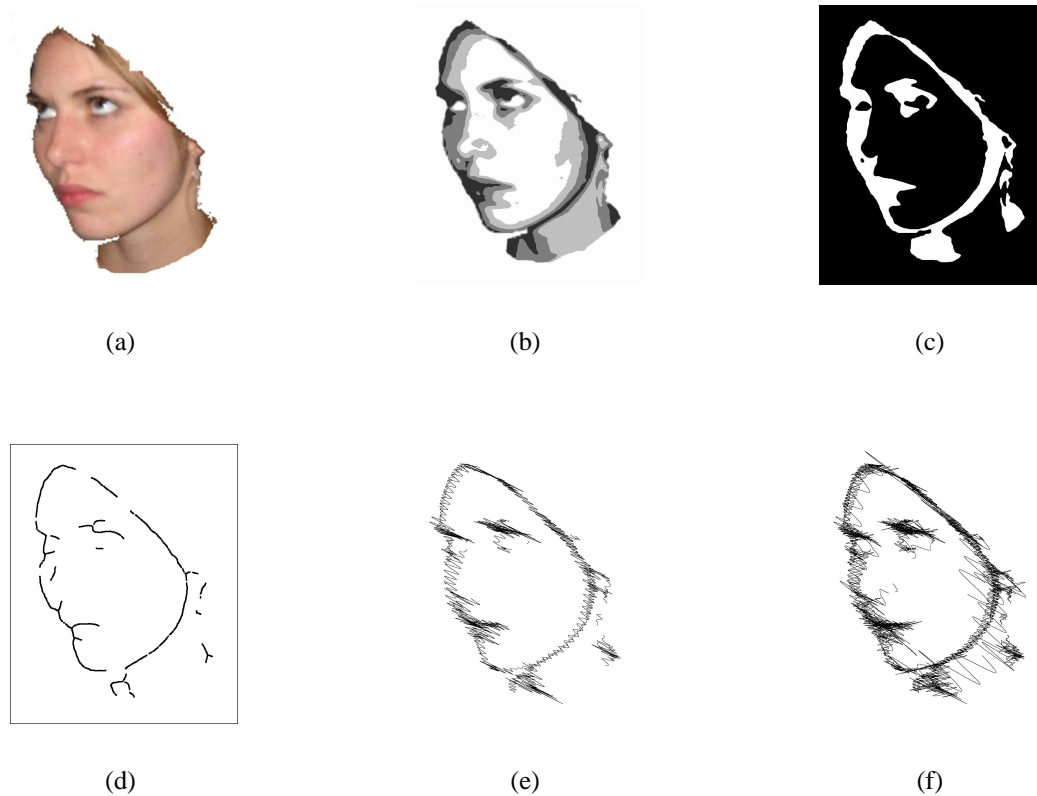


Figure 7: Example of \mathcal{MA} based sketching (adapted from [163]). (a) Automatically segmented face region, Maeliss, 2003. (b) k -means clustering after blurring. (c) Binary map representing two gray levels. (d) Approximate \mathcal{MA} map of binary map in (c). (e) Example of sketching executed using (c) and (d). (f) Example of the sketching process for four segmented levels.

Deussen *et al.* use the 3D \mathcal{MA} to provide the main axial directions from which to derive perpendicular intersection planes to draw hatching strokes on the object's surface [43].

In *sculpting*, Brower Hatcher *et al.* have developed a concept for biomimetic sculpture, *i.e.*, sculpture which either mimics living organisms (animals, plants) or incorporates in its form the influence of the environment, *e.g.*, sun exposure, rain, wind, or the proximity of humans. The resulting sculptures take the form of layered scaffoldings constituting a volumetric matrix into which smaller sculp-

tural elements can be integrated. The layering approximates a discrete 3D wave propagation [62].

The 3D \mathcal{MA} proves useful in two ways when simulating this biomimetic sculpting process. First, given an initial layer, *e.g.*, giving a description of a natural form, the \mathcal{MA} indicates the singularities for the growth, and can therefore be used to automatically either stop propagation or slow it down when near these. This is necessary to obtain a matrix which can be built and can sustain its own weight. In particular, minimal angles on the final scaffolding nodes need to be imposed (Figure 8). Second, a regular mesh for the 3D \mathcal{MA} sheets can itself serve as a set of initial layers to be grown to generate biomimetic scaffoldings [62].

7 Motion Analysis, Body Animation, Robotics

The motion analysis of human or animal (articulated) figures has been modeled by dynamic 2D \mathcal{MA} 's, *i.e.*, \mathcal{MA} 's derived from the outlines of figures in video or snapshot sequences. This representation in a skeletal form of moving figures has its roots in the works of Etienne-Jules Marey (circa 1880) when the first application of rapid photography were made to study the motion of horses, humans, *etc.* [25, p.83].

In computer graphics, for visualization purposes such as in *animation* and the simulation of movement, articulated figures have been summarized by various types of skeletons where articulations correspond to junction nodes of the \mathcal{MA} . For example, Van Overveld and Wyvill use 3D skeletons approximated with polygons and line elements; these are also used to re-render the shape (as it is animated) by “extruding” (growing) the surrounding surfaces associated to each polygonal elements of the skeleton [166]. Unwanted blending and bulging are avoided with this approach. Lazarus and Verroust use a level-set method to construct a 3D \mathcal{MA} which is akin a generalized axis cylinder representation, where a solid shape is flooded from various “sources,” and where the center of each (flooding) level set is tracked at successive layers to obtain a final curve-like 3D skeleton [174] (Figure 9). This 3D curve skeleton is then used for animation and shape deformations. A related approach is proposed by Wade and Parent who build a control skeleton for inverse kinematics (or IK skeleton) by successive discrete thinning applied to the voxelization of a 3D solid [176]. In yet another related technique, Teichmann and Teller use the 3D Voronoi diagram which is then simplified to obtain an approximation of the 3D \mathcal{MA} upon which a network of virtual springs are attached for animation purpose [157].

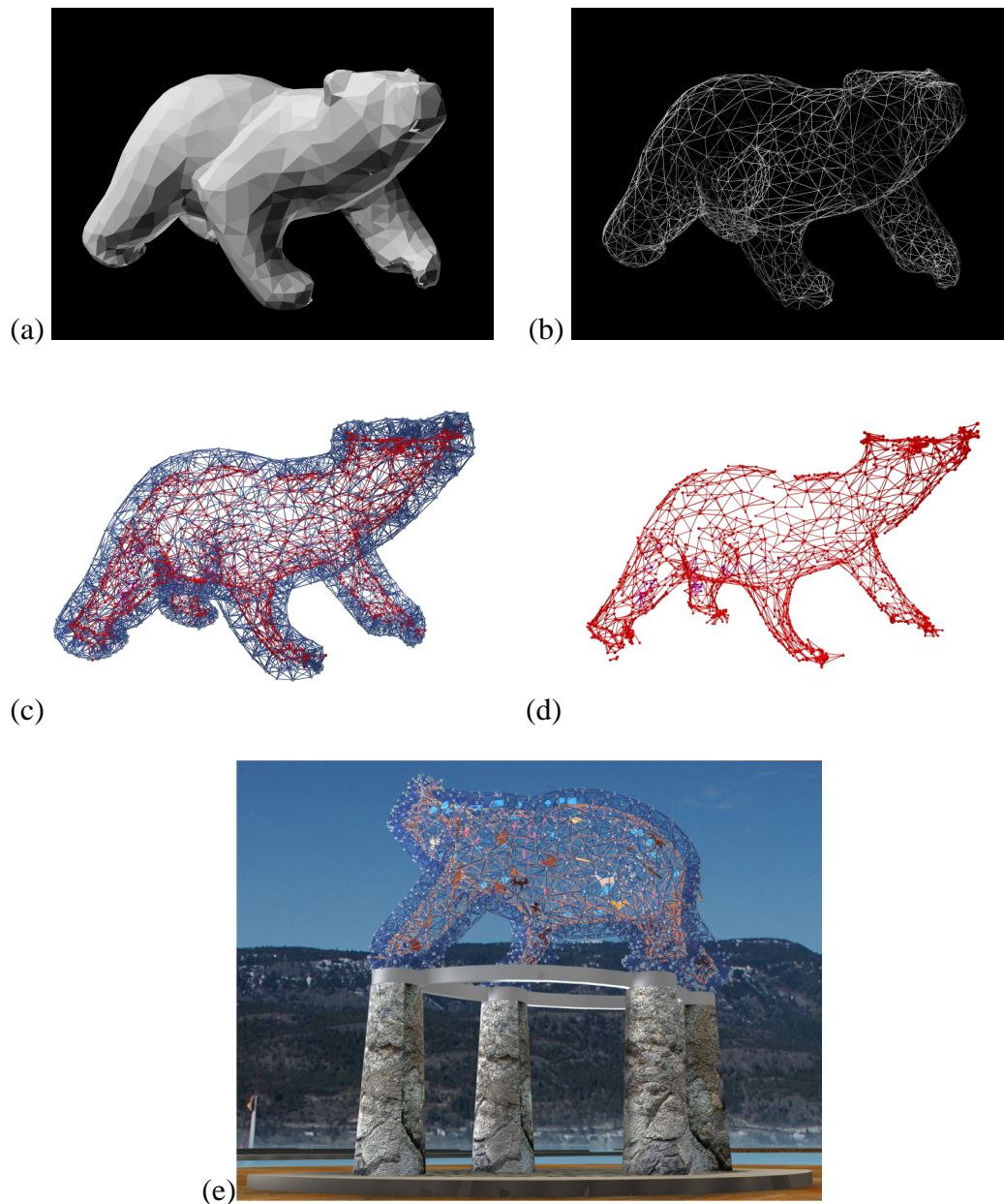


Figure 8: Production of a biomimetic sculpting using the 3D \mathcal{MA} (with permission from Brower Hatcher and Karl Aspelund of Mid-Ocean Studio, Providence, RI, USA). (a) A toy bear was laser scanned at coarse resolution to get a 3D solid rendering. (b) The wire-mesh for (a) is used as a source of propagation in 3D. (c) and (d) two steps (layers) of propagation where self-intersections are apparent in the propagation (automatically detected and avoided by the use of the 3D \mathcal{MA} [62]). (e) Final biomimetic sculpting rendered in the style of Brower Hatcher.

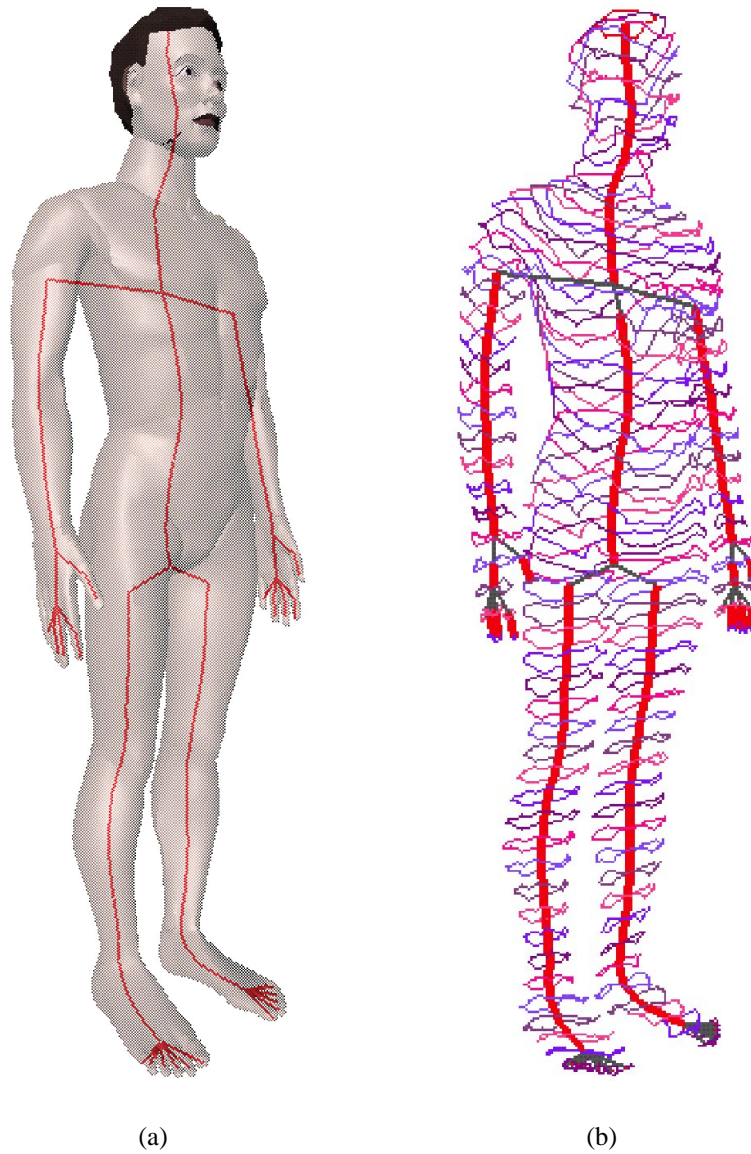


Figure 9: (Adapted from [89], with permission from the authors.) (a) Man body modeled with 15,000 faces and with the “source” of the flooding, which creates level-sets, being taken at the top of the head. (b) A “center” of each level set is selected and linked to its predecessors as to minimize the path-length to the source.

In *motion planning*, the outline of the environment, such as the floorplans of buildings, the layouts of streets, or any workspace with obstacles, is used as a constraint for which one needs to find “optimal” paths leading from a goal to a target locus, where the optimum implies a compromise between the total length and complexity of a path, and some measure of minimum distance to the obstacles or “clearance.” The moving object is often represented by its convex hull or an enveloping sphere to ensure some minimum clearance to the obstacles, and can then be considered a rigid body in motion. The \mathcal{MA} has been used in this context as a set of candidate paths ensuring the moving objects stays as far as possible from walls, pedestrian walks, corners, *etc.*, as well as being indicative of main direction flows to follow to move from one extremity of a room or corridor to another [188, 61, 69]. The \mathcal{MA} , which is used to ensure maximal clearance along a path, can also be relaxed toward the visibility graph which provides shortest linear paths with weak clearance, allowing for a possible compromise between path length, smoothness and clearance [178].

When considering articulated objects or robots, with n degrees of freedom, typically modelled as Euclidean translations and rotations at the joints, a practical method considers first a set of approximated loci sampling a high-dimensional configuration space. Such discrete paths can be efficiently computed, and usually ensure some minimum clearance, but often are far from being optimised (in length, smoothness, maximum clearance). However, an approximate path can be improved by “retracting” it to the \mathcal{MA} of the workspace [53]. Geraerts and Overmars further propose to find along this \mathcal{MA} “ridges” to maximize clearance to obstacles [54]. A “ridge” corresponds to a path on the \mathcal{MA} of the workspace such that the radius function is kept locally maximal. For example, for a 3D workspace, this will involve navigating via axial curves, where multiple \mathcal{MA} sheets intersect, or along \mathcal{MA} sheets following a gradient descent method.

8 Machining, Metal Forging, Industrial Design, Database Mining

The \mathcal{MA} implicitly defines object offsets, which are required in *numerical tool machining* applications for milling, tuning, punching and drilling [63, 64]. In addition, it has been used for surface meshing [68, 3], volume meshing and finite element analysis [138, 139, 130, 190], dimensional reduction and detail suppression [147, 103], as well as shape morphing [19], and haptic exploration of surfaces

[124, 125]. The ability of the \mathcal{MA} to implicitly represent the distance of a point to a (complex polygonal) shape is useful in dynamic path modification for rendering, collision prevention, tolerance verification, visibility computation, accurate motion dynamics and 3D path planning, and self-intersection detection.

In the simulation of the *flow of materials*, the \mathcal{MA} can be used to rapidly predict changes in patterns for complex dynamically changing geometries. For example, the 2D \mathcal{MA} has been used in metal forging to model the hot metal material constrained to move in an enclosed space. Cavities, which are invaded by the flowing metal, keep changing shape as pressure is applied [184]. At each iterative steps of a reverse process simulation, the 2D \mathcal{MA} of cross sections of the metal in that space is used as an accurate and efficient deformation predictor.

The \mathcal{MA} or some equivalent skeletal representation can be used as a tool for *shape interrogation* [130], reconstruction, modification and design, and even as a basic element for building intuitive new interfaces for *shape modelers* [7, 18, 189, 190] (Figure 10). Using a 3D skeleton as the underlying shape representation gives the designer greater capacity to impose in unison geometric and topological constraints on a shape model, to attach functional representations to different parts of the model, and to specify non-uniform material distribution via offsets [161].

Shape identification, for the purpose of detection, classification, and recognition, permits to *search* very large databases of 2D and 3D objects and has applications in many fields, such as medical information management systems, surveillance and security (*e.g.*, the identification of people), object archiving (*e.g.*, for museums) [75, 16]. An important step in creating a generic solution for shape identification consists in solving the “global registration” problem, *i.e.*, identifying an optimal alignment between two fragments of 2D/3D objects. In 2D, Siddiqi, Kimia *et al.* address this problem by using a shock graph [149, 151, 143, 144]. In 3D, Leymarie, Kimia *et al.* use a medial scaffold, a compact hierarchical 3D graph version of the \mathcal{MA} [101, 105, 32, 103]. The hierarchical nature of these compact graphs permits to simplify the representation of a given object by ordering shape features via a notion of scale. In combination with transitions under perturbations or deformations, smaller, less significant features can be removed before attempting a matching procedure [158, 103]. Then, the more significant part of a shock graph, in 2D (Figure 11), or a medial scaffold, in 3D (Figure 12), is used to be matched with a template or other target graphs.

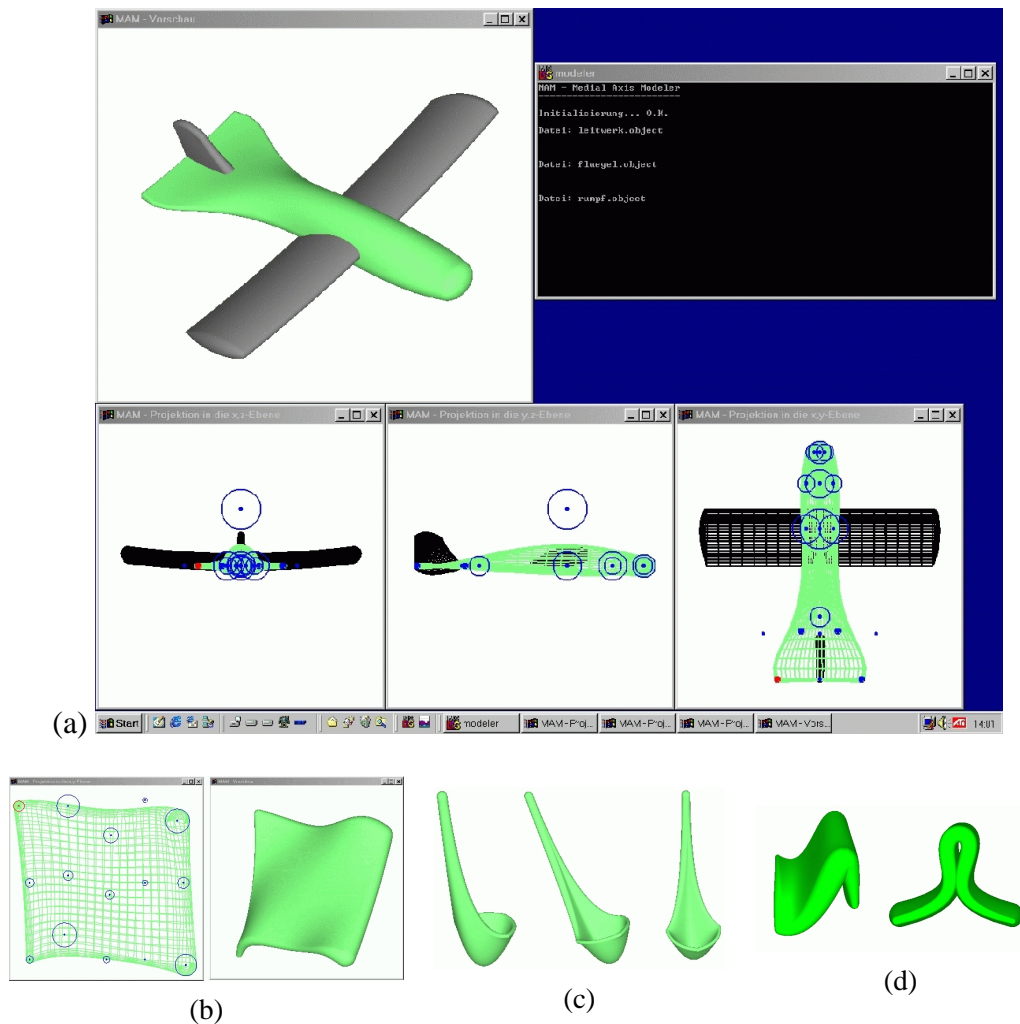


Figure 10: (a) *Modeler* based on the notion of 3D \mathcal{MA} (with permission from Franz-Erich Wolter). The boundaries of the generated objects are the envelope surface of maximal spheres whose centers are located on the \mathcal{MA} surface. These examples illustrate that it is possible to create, and modify, the shape of solid objects in an intuitive and systematic manner by modifying the maximal disc radius function associated with the initial \mathcal{MA} . (b) Growing or shrinking of the maximal disc radius function results in the solid's growing or shrinking, respectively. (c) Example of a “spoon”-like solid with concave and convex bounding surfaces. (d) Self-intersections occur if the maximal disc radius is not properly controlled during the construction of the envelope surface supposed to bound the newly designed solid. A careful treatment of the 3D \mathcal{MA} permits to control and avoid this problem.

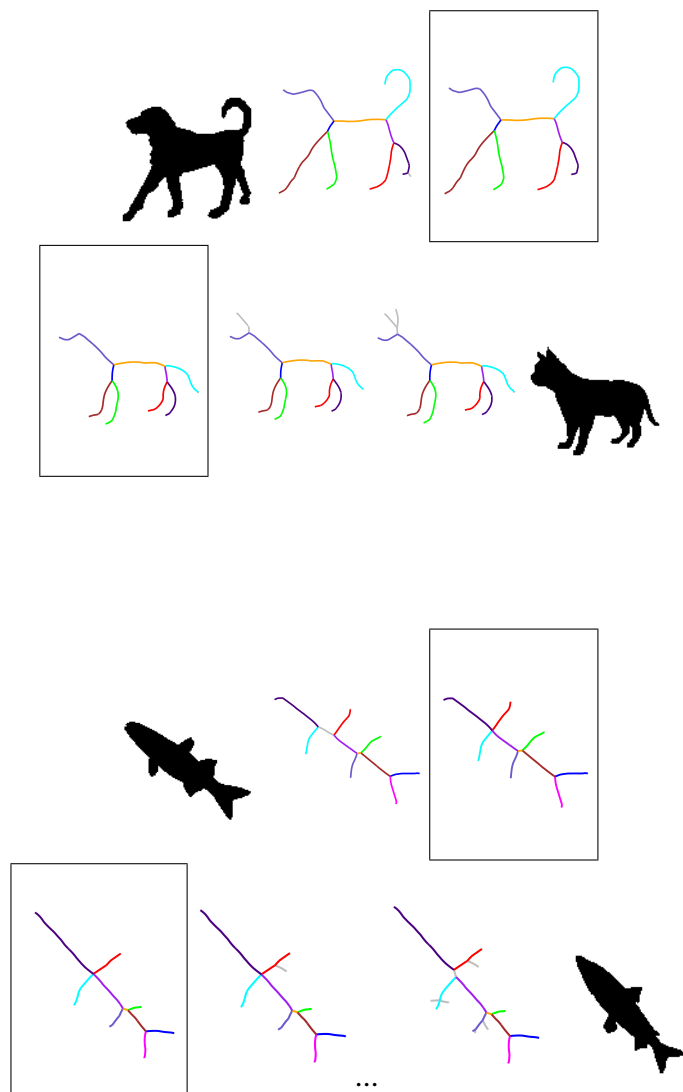


Figure 11: (Adapted from [144].) Examples of the optimal deformation path between two shapes represented at the extremes of two sequences (here between a dog and a cat at the top, and two different fishes at the bottom; . Each sequence shows operations (symmetry transforms) applied to the \mathcal{MA} , and the resulting intermediate shock graphs. The boxed shock graphs which have the same topology, are where the deformation of the two shapes meet in a common simpler shape.

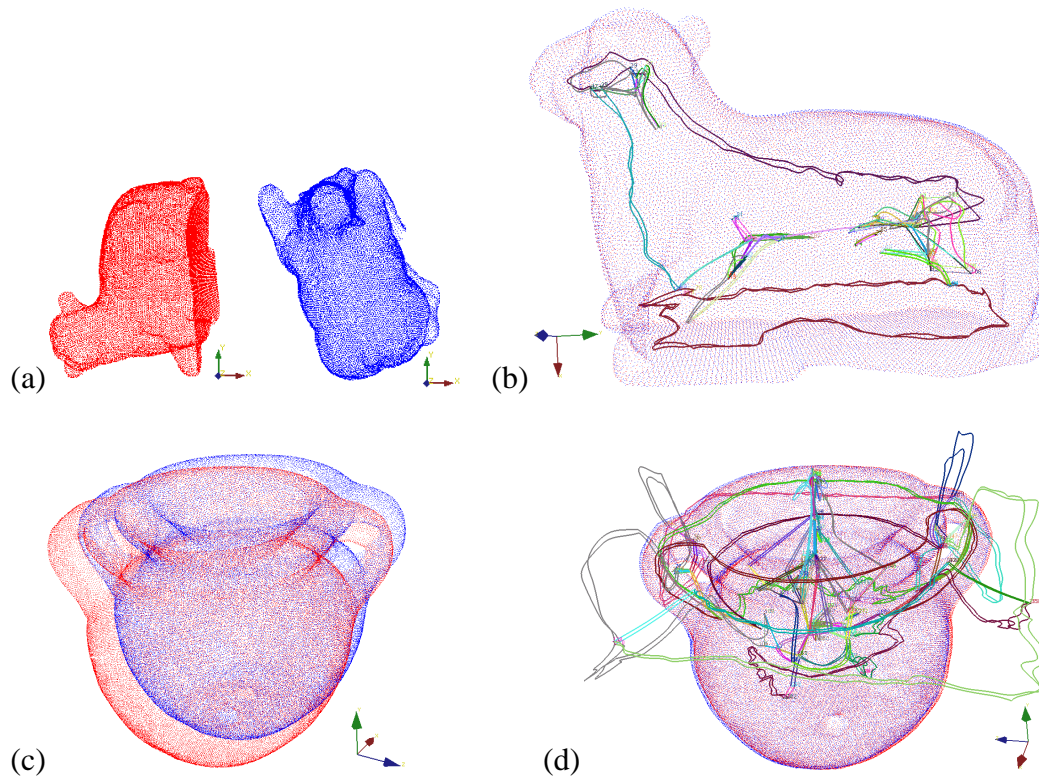


Figure 12: (Adapted from [32].) This figure illustrates how the medial scaffold can be used for registering two scans of a 3D object obtained at the same resolution (20K points) by two distinct operators. (a) The “sheep object” from two scans with different viewpoints. (b) The registration result. Matched links are colored in pair; unmatched ones are drawn in gray. (c) An archaeological pot under two scans. Note that due to range scanner capability, the data has holes. (d) The registration result.

9 Medicine and Biology

One of the first intended domain of application for the \mathcal{MA} was in the areas of medicine and biology. Harry Blum conceived of the 2D \mathcal{MA} as a natural descriptor for shapes such as cells and body tissues, as well as entire anthropomorphic bodies or sub-parts, such as the arm, hand and fingers. His main manuscript was published in the Journal of Theoretical Biology [21]. We mention below some of the main areas of application of the \mathcal{MA} in medicine and biology illustrative of the possibilities it offers.

Image and Object Segmentation Sebastian *et al.* have introduced the idea of using the 2D \mathcal{MA} to modulate the “competition” between nearby deformable contours when segmenting noisy image data with tissues coming in close proximity [145]. The 2D \mathcal{MA} positioned as an inter-region skeleton acts a “predictor of boundaries” in a feedback loop with the deformable curve models. Each curve model is grown and deformed from an initial “seed” region (either manually or automatically). This method leads to improved bone segmentation of the wrist and spine regions [39]. Images of bones are often hard to segment because of: (i) the varying densities observed in the bone structure (the outer layer or cortical bone being denser than the spongy bone tissue it encases), and, (ii) the close proximity of separate bones part of closely integrated articulated structures, where successive or coupled bones form complex 3D architectures. Sebastian *et al.* use the result of segmenting successive CT scans to isolate profiles, which can then be connected to reconstruct in 3D each carpal bones of the wrist [145].

Path Planning and Virtual Endoscopy The 3D \mathcal{MA} of solid objects representing tissues can be used to generate central paths to help simulate navigation in the human body without approaching too closely the tissue boundaries.¹⁵ This is helpful for example to plan probes insertion, or visualize the 3D navigation through vascular regions, the colon, the lungs, and so on. Zhou *et al.* compute a discrete 3D \mathcal{MA} from a voxelisation of medical imaging sensing data (CT, MRI) [192]. They then compute various paths along the resulting 3D \mathcal{MA} following voxels with local maximal distance (*i.e.*, maximizing the radius of the associated maximal contact sphere). A similar method based on the 3D \mathcal{MA} is used by Paik *et al.* for virtual endoscopy where a central path is obtained more directly and robustly by the use of a shortest path constraint between a source and sink for each branch

¹⁵In similitude to the motion planning problem of robotics (§7).

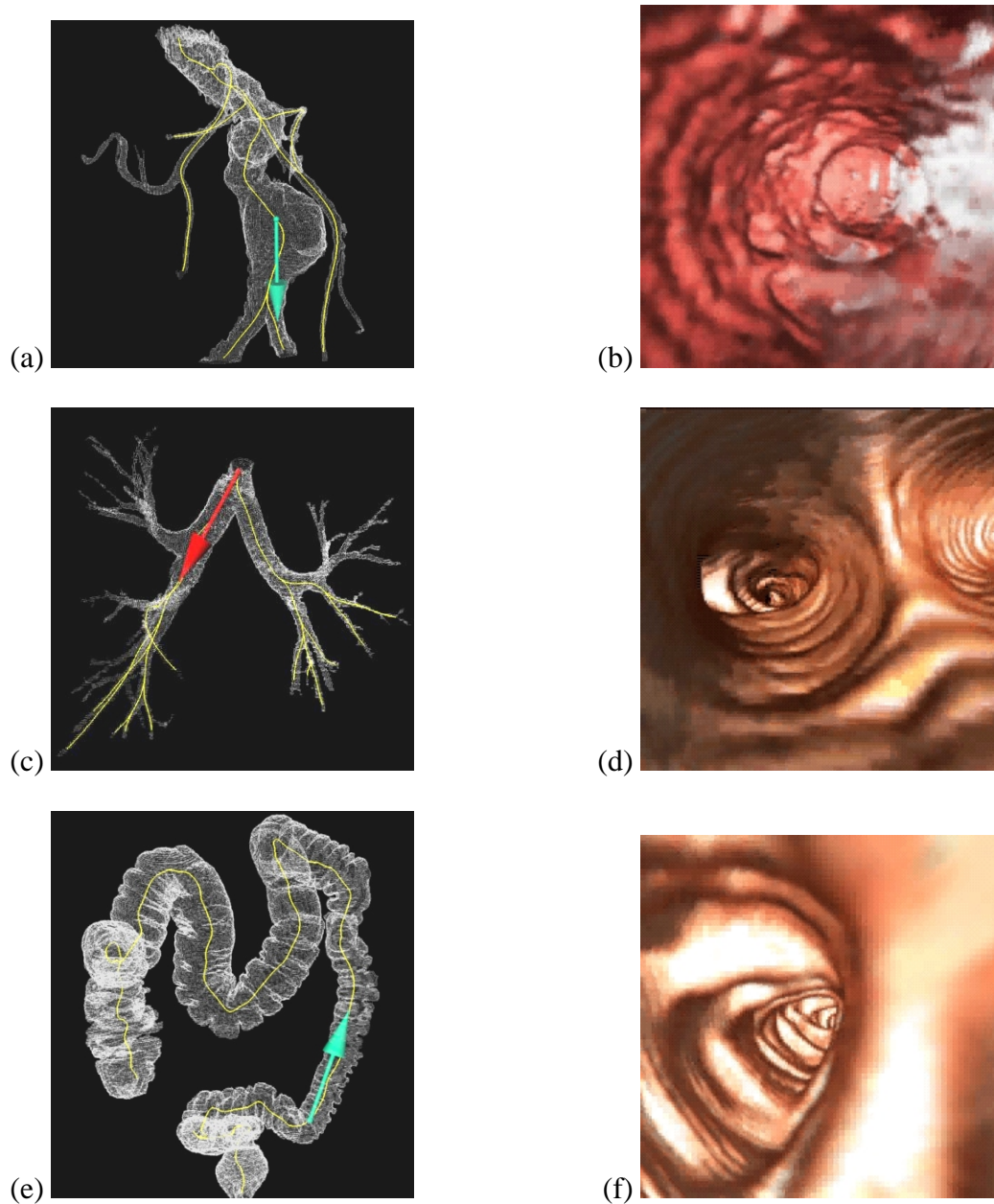


Figure 13: (Adapted from [126], with permission from D. Paik.) (a) Aorta and virtual camera pose along the computed path. (b) One shot of the virtual angiography sequence produced for the aorta in (a). (c) Bronchi and virtual camera pose along the computed path. (d) One shot of the virtual bronchoscopy sequence produced for the bronchi in (c). (e) Colon and virtual camera pose along the computed path. (f) One shot of the virtual colonoscopy sequence produced for the colon in (e).

to be navigated along [126] (Figure 13). Kaufman *et al.* improve on the detection of sources and sinks and the use of distance fields to smooth centerline paths for virtual camera navigation [17, 177].

Morphometry, Branching Tree-like Structures Mangin *et al.* since the early 1990's have been developing an approach to the study of brain data (typically obtained from MRI scanners) emphasizing the morphometry of large structures, in particular the intricate folds delimiting the 3D pattern of the surface of the cortex, called *brain sulci*. Their methodology depends on the use of the 3D \mathcal{MA} . They compute a discrete 3D skeleton of the cortex with erosions¹⁶ being performed at varying speed to reflect the influence of various “materials” and thickness. This permits for example to better localize the ribs of the skeleton in the depths of crevasses where cerebro spinal fluid is present. Homotopy¹⁷ is imposed in the erosion process, to fill-in possible holes in the original dataset, so that the resulting form preserves the ideal spherical topology of the cortex. Ribs of the computed 3D \mathcal{MA} are then used to create a 3D graph representation of the folds (or brain sulci; Figure 14). Brain morphometry understanding is believed to be key to study “neuroanatomical structures which may be preferentially modified by particular cognitive skills or diseases” [113].

A fundamental geometric structure found in all pluricellular living organisms takes the form of *space-filling tree-like branching shapes* that support both plants — roots, trunk, branches and leaves — and animals — vascular blood systems, bronchial tree of the lungs, epithelial ducts of the prostate gland, ureteric tree of the kidneys, and so on; for example, a normal human kidney contains between 300,000 and 1 million “nephrons:” *i.e.*, tips of branches of the ureteric tree [40]. A practical way to study such complex branching structures is to represent them as 3D graphs via a 3D \mathcal{MA} . Jeulin *et al.* use a 3D thinning technique to capture the fine branching structure of mouse kidneys imaged with laser scanning confocal microscopy [40, 29]. They use the resulting 3D \mathcal{MA} to measure the lengths of individual ureteric branches and the total length of the ureteric tree. Chaturvedi and Lee also use a 3D thinning process to obtain a 3D skeleton of the airway structure for the lungs of small animals [34]. This skeleton is then used to represent the bronchial tree structure which serves in morphometric studies over multiple

¹⁶In the sense of Mathematical Morphology operations, representing a discrete wave propagation or thinning process [146, 152].

¹⁷Two (mathematical) objects are said to be homotopic if one can be continuously deformed into the other (after Henri Poincaré, circa 1900 [35]).

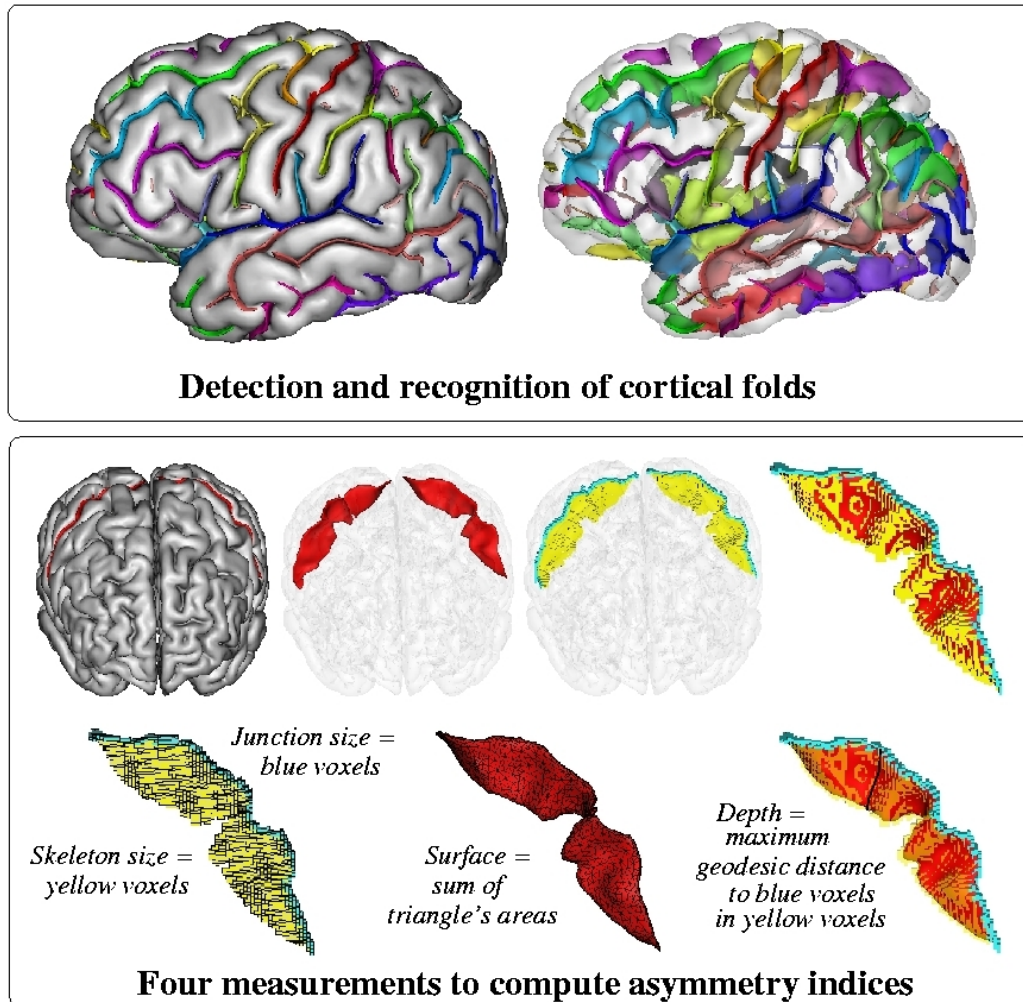


Figure 14: (Adapted from [113, Fig. 4], with permission from J.-F. Mangin.) Top: Cortical folds are represented by computing a 3D \mathcal{MA} using an erosion process acting on the deep crevasses. Bottom: Each cortical fold is then further characterized by four quantities.

generations. Sanniti di Baja *et al.* use a version of the 3D thinning of volumetric images to obtain a 3D curve skeleton of the blood vascular system from angiographic images [122, 154].

Growth, Form Genesis The 3D \mathcal{MA} can also be used to study growth problems in embryology. For example, Mangin *et al.* propose that further understanding shall be gained by “studying the cortical folding process during brain growth” [113]. Āurikovič *et al.* use the \mathcal{MA} to represent the brain of an embryo in the womb, from key frames of a video sequence [41], where the \mathcal{MA} is interpolated between key frames to produce additional renderings, by re-growing the shape according to the associated radius function of the \mathcal{MA} , in order to obtain smoother visual effects when producing the final animation. They use a similar approach to study other organs’ growth, such as for the stomach and the intestine [47]. They combine the \mathcal{MA} with an L-system (typically used to model plants) to capture the topology of the entire digestive system represented as a tree structure [46]. Jeulin *et al.* study the growth of kidneys’ ureteric trees modeled by a 3D \mathcal{MA} in a population of mice. The length distributions of the ureteric trees for different growth periods indicate “the existence of a programmed pattern of ureteric branching and growth” [40].

Deformation and Motion of Cells Leymarie and Levine use the 2D \mathcal{MA} as a shape descriptor of live cells to represent the deformation of their boundary, and in particular make prediction of growths of pseudopods of neutrophils, known to use these to move in their environment [99, 100]. As a branch of the \mathcal{MA} grows (or shrinks), their system makes the prediction that the region at the tip of this branch (at the front, if growing, or behind, if shrinking) can be used to restrict the tracing of deformations of the boundary of the cell. In particular, this permits to make the cell tracking system more robust to rapid or discrete changes and motions.¹⁸

Recognition: From Tissues to Cellular material For the purpose of the object recognition of body tissues, the 3D \mathcal{MA} has been proposed as a potentially useful representation. Székely *et al.* developed an algorithm for approximating the 3D \mathcal{MA} of a cloud of points sampling the surface of a tissue [155, 121]. Steps toward

¹⁸Leymarie and Levine call their growing and shrinking \mathcal{MA} “dynamic skeletons;” these represent a particular implementation of the concept of Process Inferring Symmetry Axis (or PISA) of Leyton [107] where the tip of significant \mathcal{MA} branches are constrained to be attached to the associated local curvature extrema of the cell outline.

the goal of Székely *et al.* of shape matching have been achieved by Chang *et al.* on the basis of the medial scaffold, a graph representation of the 3D \mathcal{MA} [32] (Figure 12 in §8 gives two examples in other domains at the scale of human tissues). Pizer *et al.* have explored since the early 1980's a number of medial representations for shape characterisation, and have promoted their use to model 3D “medical forms:” human tissues, vascular networks, bones, and so on [133, 132, 153]. Attali *et al.* characterise, via a 3D graph structure built from a Voronoi diagram, the shape of complex elements such as a vertebra or a chromosome [9, 48].

Beil *et al.* study dynamics of the keratin filament network part of the cytoskeleton of epithelial cells. Such a network structure is key in the formation of a scaffold defining the shape and mechanical properties of cells [15]. Beil *et al.* map the 2D \mathcal{MA} of electron microscopy images of regions of human pancreatic cancerous cells to a graph structure. Such graphs can then be studied under deformations, *e.g.*, during cell migration.

Bajaj *et al.* propose to process cellular material from molecular tomographic imaging to study, characterise and recognise “cellular machines” built from hundreds of individual proteins [12]. Different structural arrangements of these proteins lead to different “machines” which can efficiently carry out their physiological functions. The 3D \mathcal{MA} is used to simplify the data while retaining important structural features useful to compare different multi-protein cellular complexes. Bajaj *et al.* construct a graph version of the 3D \mathcal{MA} by directly linking critical points of the 3D tomographic images seen as density fields.¹⁹ Such a 3D graph can also be used to study and visualise plant and animal viruses from data obtained via electron microscopy [11].

10 Crystallography, Chemistry, Molecular Design

At scales smaller than what is typical of medical and biological problems, we reach the molecular and atomic structure of matter. At that level, 3D graph structures — which make explicit the topology of the networks connecting atoms to form molecules — are a favored representation. In crystallography they are called “critical nets,” while in computational chemistry they are usually called “molecu-

¹⁹This is based on the notion of a critical graph of a Morse function, which is closely related to the 3D medial scaffold [101] (which maps the 3D \mathcal{MA} to a graph) and to Reeb graphs [65] (which characterise the topology of level sets). *Critical points* of a function f on a manifold M are found where the gradient vanishes, *i.e.*, $\nabla f = 0$. Such a function is said to be “Morse” if its critical point are non-degenerate, *i.e.*, they are isolated.

lar graphs.”

Diffraction data from X-ray crystallography reveals individual atoms in electron density maps. X-rays have the proper wavelength (in the Ångström range, *i.e.*, $\approx 10^{-10}$ meter) to be scattered by the electron cloud of an atom of comparable size. At high enough resolutions, typically for less than 2.5–3.5 Å., a stick model may be directly fit to the 3D data where atoms are well isolated, although this usually involves human interaction. Whether at such high resolution or lower ones, an automatic processing of the data is desirable to identify the “backbone” or 3D skeleton of a potential stick model.

A common practical method to retrieve such structures consists in applying an erosion process to the 3D electronic density field capturing the shape of the space occupied by a molecule or a set of atoms. The 3D skeletonization of electron density maps is a popular method, dating back to the early 1970’s and refined since, which is used to automate the tracing of the molecular chains linking different atomic centers [59, 60, 74, 4, 135, 58]. This method first segments a useful volume enclosing the atoms or molecules of interest, which can then be thinned down to retrieve an approximate 3D \mathcal{MA} from which the skeleton is derived. In its simplest form, the segmentation is based on selecting an iso-surface of the electronic density field (Figure 15).

Based on the quantum theory for atoms [10], a direct construction of the molecular graph is also possible. Critical points of either (*i*) the 3D \mathcal{MA} obtained from the above thinning process of an iso-surface [109],²⁰ or (*ii*) a gradient field derived from the electron density map [92, 12], become nodes of the graph structure.

At lower resolutions which are common in practice, *i.e.*, for more than 2 Å, or for low quality electron density maps, the points of maximum density do not always correspond to isosurface centers, preventing accurate positioning of the final stick model. A solution to this problem has been proposed by Aishima *et al.* starting from the 3D \mathcal{MA} of iso-surface segments of the electron density map [2]. An approximate \mathcal{MA} using the *power crust* method of Amenta *et al.* [5, 4] is thinned down to create a 3D graph. Points of this thin approximate \mathcal{MA} are then matched to atoms of a ligand model, *i.e.*, an existing molecular model. Aishima *et al.* report that this \mathcal{MA} -based method is at least as powerful as critical point graphs at high resolution, and looks promising for applications at lower resolutions.

Once a reliable molecular graph is obtained, various applications are possible,

²⁰This is closely related to the medial scaffold representation [101].

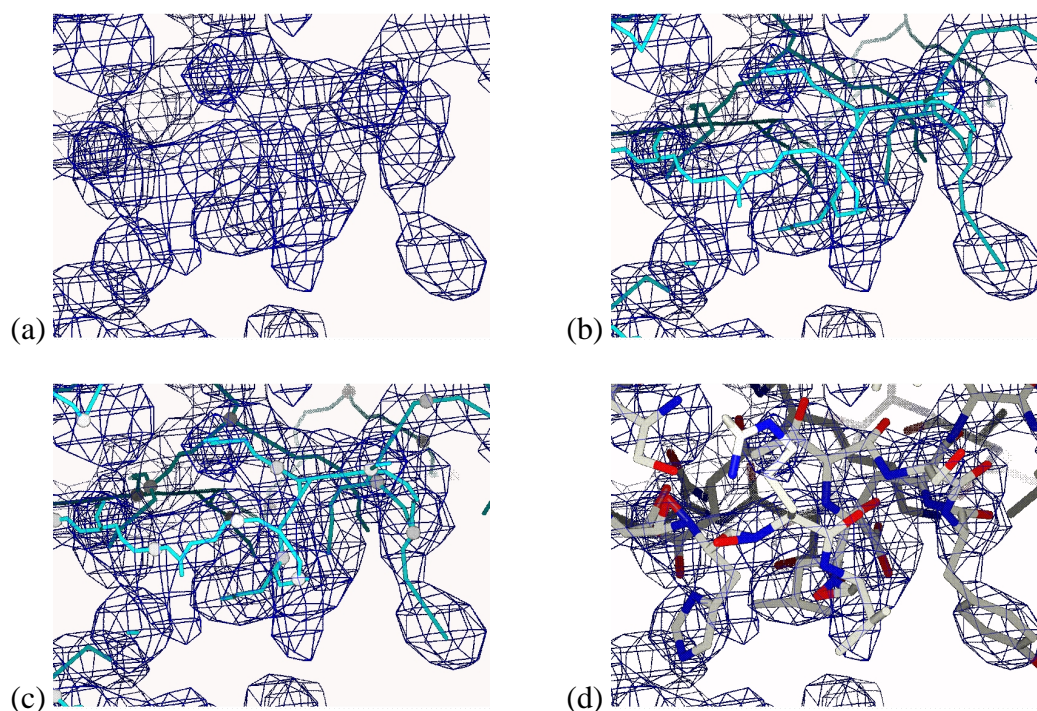


Figure 15: Illustration of the 3D skeletonization of an electron density map to produce a backbone for a molecular graph; figures provided by Thomas Ioerger *et al.* (adapted from [58] with permission from the authors). (a) Typical electron density map around a protein; the density map is generated from x-ray crystallography data. (b) The trace points are essentially along the \mathcal{MA} of the density. (c) Chains are shown that connect some trace points (that are putative carbon-alpha atoms), and represents the "backbone" of the protein. (d) The 3D structure of the protein at atomic level, derived from the trace and chains, is shown, where different inter-atomic bonds are in various colors.

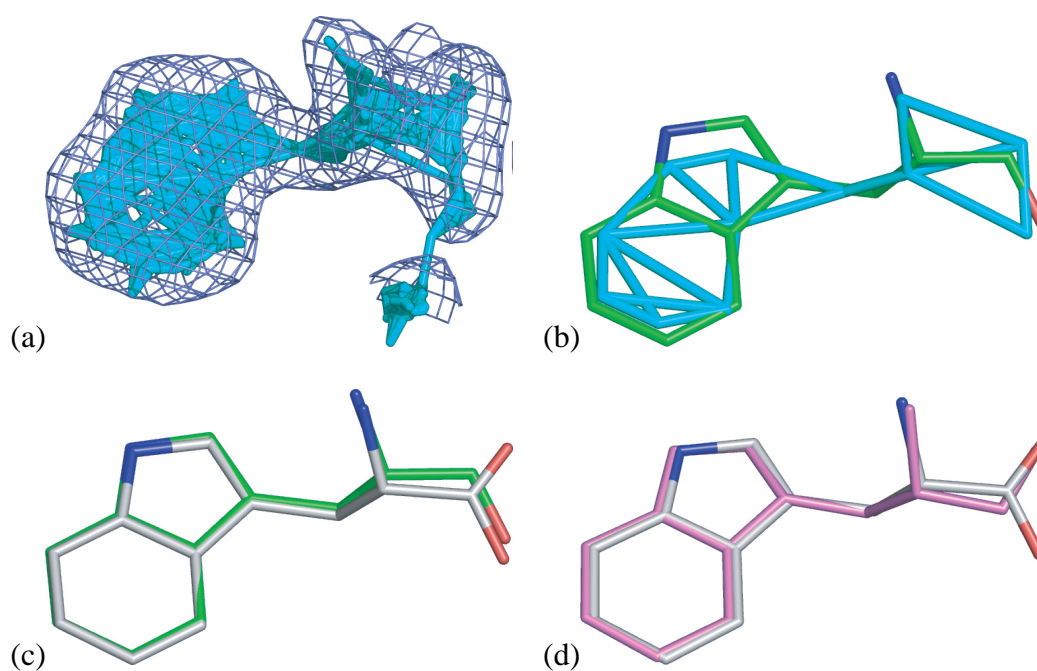


Figure 16: (Adapted from the work of Brunger *et al.* [2, Fig. 4], with permission from the authors.) Electron-density map for a tryptophan ligand bound to anthranilate synthase. (a) Prior to thinning, the full \mathcal{MA} (cyan) is a wide flat shape inside the isosurface (blue mesh). Both the full \mathcal{MA} and individual \mathcal{MA} segments are too complex for direct graph matching against ligand-coordinate graphs. After thinning the \mathcal{MA} by using “simplify” from the Power Crust software package [5], the \mathcal{MA} is converted to edges and vertices and thinned to obtain vertices (cyan) separated by approximately atom-to-atom distances. (b) The thinned \mathcal{MA} (cyan) has many vertices near the atom positions from the best available ligand model (green). (c) The best model (green) aligns well with the deposited structure (gray). (d) The ARP/wARP model (magenta) also aligns well with the deposited structure (gray).

such as pharmaceutical structure-based drug-discovery efforts. In drug design, the \mathcal{MA} is a suitable substrate for building molecular surfaces and volumes [33], modeling interface surfaces of protein-protein complexes [13], modeling receptor sites and the docking of ligands inside protein cavities [94], identifying geometric invariance among molecules exhibiting similar activity, mining databases, all key geometric problems in this field [36, 22, 110, 129, 50, 70].

11 Perception and Cognition

The “scales” at which perceptual phenomena take place with the support of our brain remain to be firmly established. While the debate is open we shall consider this range of scales to be abstract, immaterial.

Arnheim, a student of the Gestalt school of perception, defines “psychological forces” as an interplay of directed tensions, having magnitude and direction, inherent in any percept. In essence, according to Gestalt theory [81, 83, 180], any percept (visual, auditory, tactile) is represented via a dense vector field. Arnheim characterizes the lines of equilibrium of forces with the notion of “structural skeleton.” The percept is seen as a continuous field of forces. It is a dynamic landscape, in which lines (of the structural skeleton) are ridges being the centers of attractive and repulsive forces, whose influence extends through their surroundings, inside and outside the boundaries of a figure; this is Blum’s \mathcal{MA} in disguise (see §6). The structural skeleton serves as a frame of reference by helping determine the role of each pictorial element within the balance system of the whole. Arnheim partly justifies the definition of the structural skeleton based on early studies in humans of dynamic sensitivity maps, where a movable dark disk on a white canvas generates preferred directions where to move next: the “directional tendency” cluster along principal axes of the structural skeleton [8, pp.14-15; Fig. 4].

Kovács, Julesz and Feher have derived differential contrast sensitivity maps for 2D shapes which are consistent with a medial function (called D-function) representing the percentage of boundary points equidistant from the observation point within a tolerance of ε (Figure 17) [85, 86, 84]. This lead them to hypothesize a medial \mathcal{MA} -based shape processing method for human vision, as originally proposed by Blum [21]. This D-function makes explicit certain medial points along the \mathcal{MA} , predicting where contrast sensitivity should be maximal, and potentially leading to a more compact representation.

The Hybrid Symmetry Transformation (HST; §5), which permits to tune the wave propagation model from Blum’s \mathcal{MA} to the more general model of geomet-

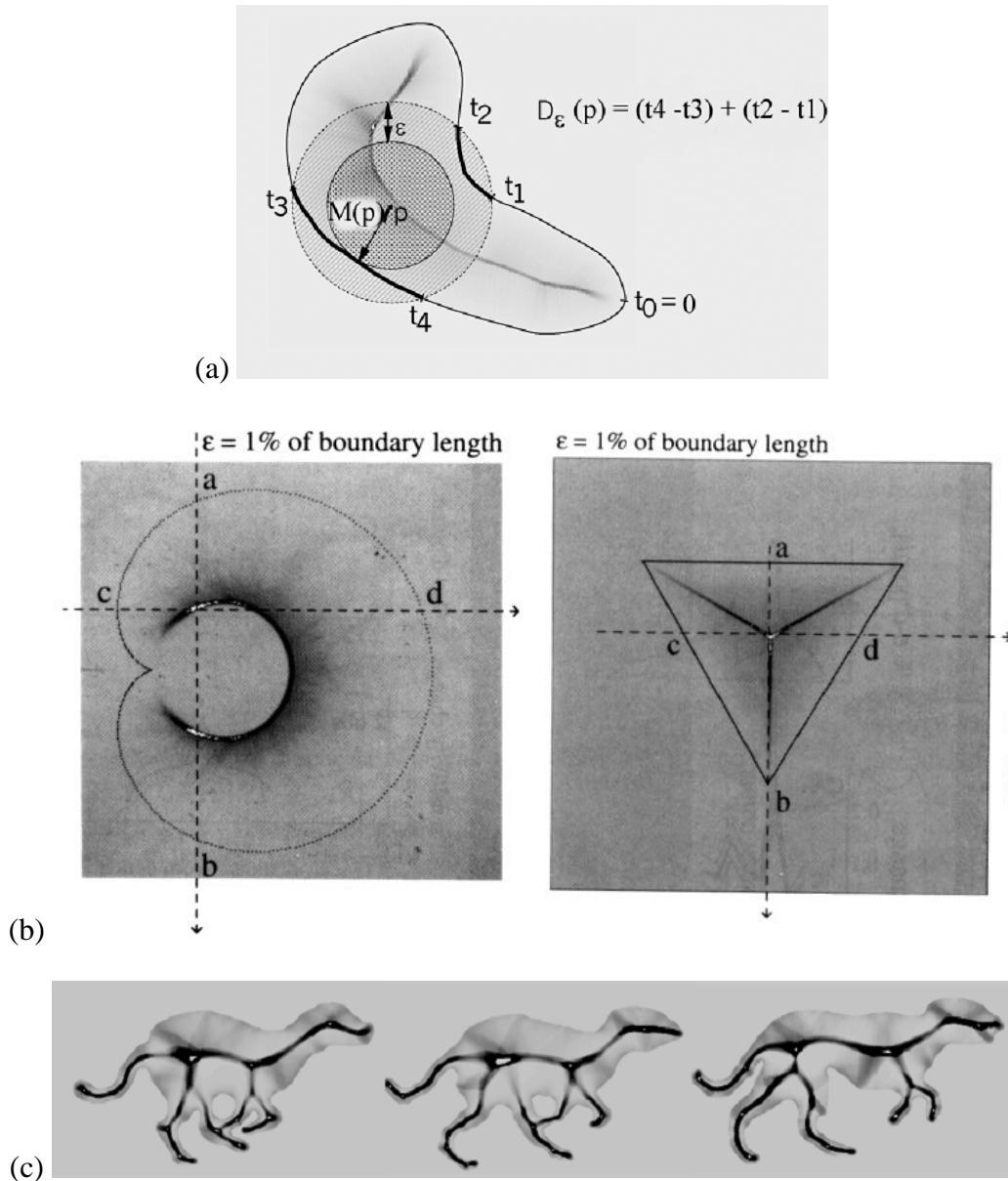


Figure 17: (Adapted from [84, Fig. 2, 8, 9 & 10], with permission from Ilona Kovács.) (a) The D_ϵ function within a simple shape is obtained as the sum of the curve segments falling within the ϵ neighborhood of the $M(\rho)$ radius circle around p . Dark shading corresponds to increasing values of D_ϵ and the “white spot” denotes its maximum. (b) Medial (“D”) function predicting differential contrast sensitivity maps, *i.e.*, predicting where contrast sensitivity improvements, involving higher activity in the primary visual cortex, are maximal, given a contour — here a cardioid on the left and a triangle on the right; cross-sections through maximum loci are indicated as dotted lines a-b and c-d. (c) The D_ϵ function for a few frames in a sequence depicting the movement of an animal. Kovács *et al.* suggest that the maxima of the D_ϵ function “are good candidates as primitives for biological motion computations” [84, Fig. 10].

ric optics — where waves can intersect, thus generating a full symmetry set — has been applied by van Tonder *et al.* with a certain success in image segmentation [170], leading to a deeper understanding of texture perception and texton theory [169]. Figure 18: 1C and 1D, demonstrate some results; a schematic of the segmentation model, called the “patchwork engine,” is also given.

The computational scheme of Kimia *et al.* based on shock graphs (in 2D) and scaffolds (in 3D) supports the speculation of Kovács *et al.* that a “sparse skeleton representation of shape is generated early in visual processing” [80]. Kimia *et al.* extend the traditional model of the \mathcal{MA} to represent images, where each \mathcal{MA} segment models a region of the image and is called a *visual fragment* (Figure 19). They present a unified theory of perceptual grouping and object recognition where through various sequences of transformations of the \mathcal{MA} representation, visual fragments are grouped in various configurations to form object hypotheses, are related to stored models, and are also consistent with the formation of illusory contours (Figure 20) [156].

12 Conclusion

“To gaze is to think.” — Salvador Dali

In this chapter we covered a spectrum of applications of medial symmetries of shape from the infinitely large toward the infinitely small. We started with a dynamic model of the formation and evolution of galaxies. We then moved on to the description of geographical information at the scale of regions of planet Earth. The representation of cities, buildings, archaeological artefacts was next, followed by the perception of gardens, and the generation of virtual plants. Having reached the scale of human activities, we followed-on with the perception and generation of artistic creations, the study of motion and the generation of animated virtual objects, and the representation of geometrically complex systems in machining, metal forging, object design. We then “entered” the human body itself with applications in medical imaging and biology. This was followed by the representation of molecular structures in computational chemistry and crystallography. Our final stop was to consider the abstract scale of the perception of visual information.

An exhaustive reporting on all recent applications of medial symmetries of shape was not the aim here. Rather, we probed into a number of domains, thus providing an “overview” meant to demonstrate how medial symmetries of shape can form the basis of a geometric language powerful enough to capture the rep-

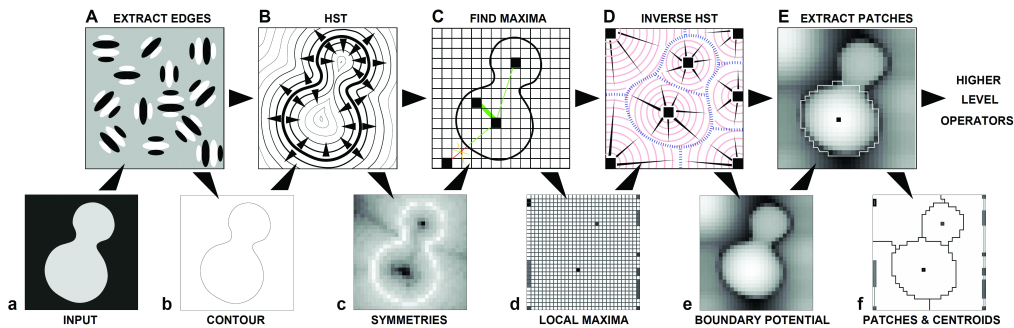
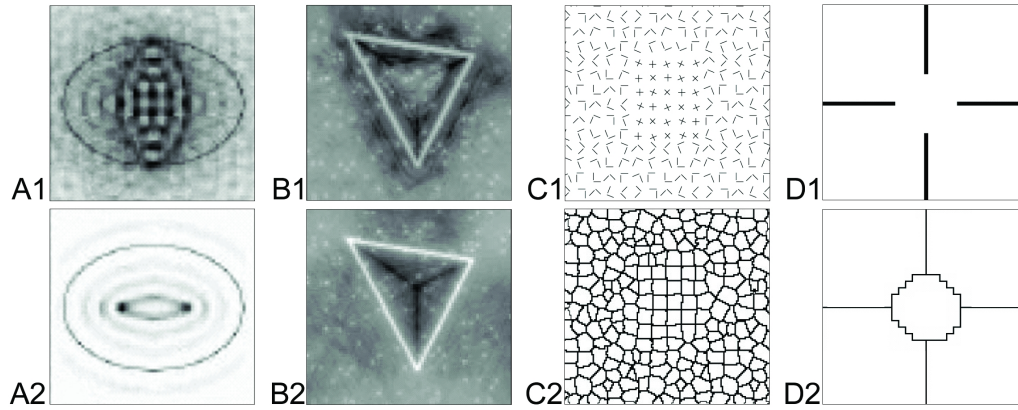


Figure 18: (Reproduced with permission from G. van Tonder) Top: HST output for an elliptical boundary contour, using, in A1, a classical wave propagation ($\nu = 0$, where ν denotes a “shunting” strength [171]), and, in A2, a blocking wave operation ($\nu \gg 1$). Only every fourth scan ring has been incorporated in the computation, to illustrate the analogy between this method and classical wave dynamics. A1 resembles waves propagating from an elliptical source in water. Strong blocking wave mode ($\nu = 3$) renders the computation sensitive to noise elements in B1 but more global medial axes are promoted in B2 in an intermediate wave propagation mode ($\nu = 0.01$). Forward-inverse HST can be used to segment various types of edge maps. For example, a texture map in C1 is segmented into a cell grid in C2, and some cases of incomplete contours are segmented into meaningful parts, such as the Ehrenstein (“sun-illusion”) figure in D1 and D2 (here computed at low resolution). Bottom: Schematic explanation of the Patchwork Engine [170].



Figure 19: Using the edge map associated with an image, visual fragments are defined and are used as canonical elements for perceptual grouping [156]. From top-left to bottom-right: (i) a grayscale image with its superimposed contour map, (ii) its shock graph, (iii) the associated visual fragments, (iv) an average intensity reconstruction of the image from the visual fragments, and (v) the resulting visual fragments after applying a sequence of selected transformations mimicking a process of perceptual grouping.

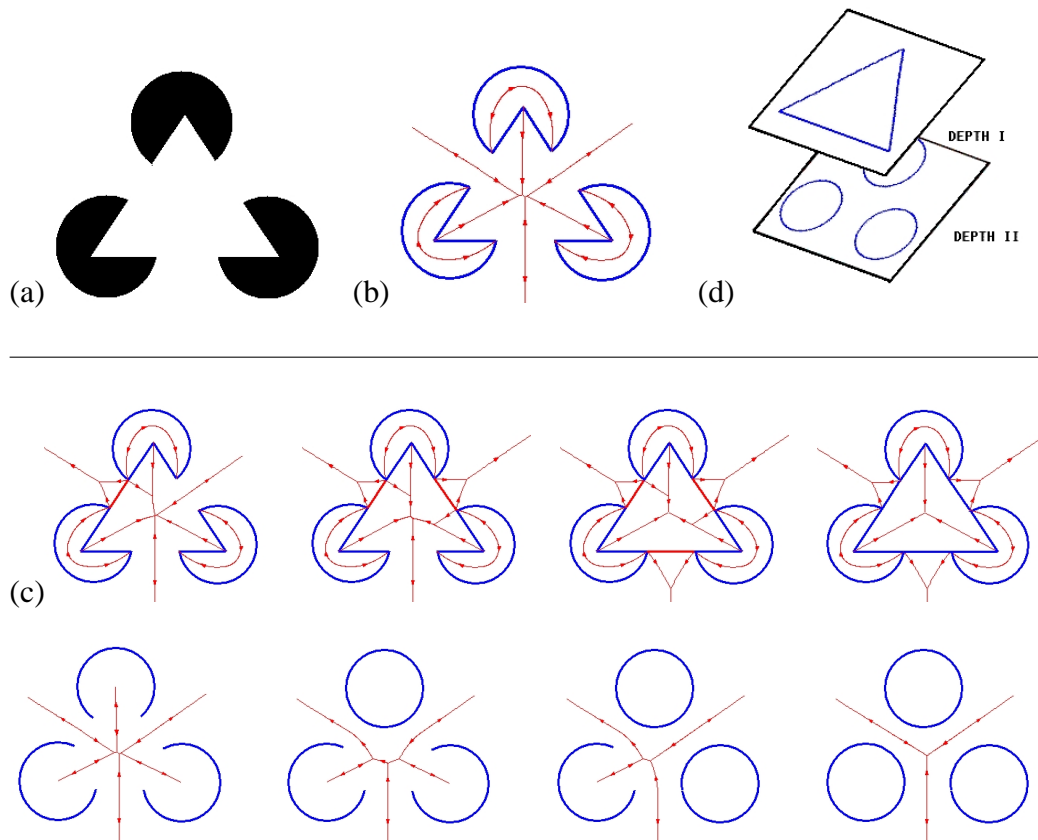


Figure 20: (From [80]) (a) The Kanisza triangle [77]. (b) The shock graph arising from the edge map. (c) This edge map can be transformed (edge elements removed, gaps bridged, and so on) in any arbitrary sequence: any transformation sequence of the edge map can be implemented by a corresponding sequence of symmetry transforms on the \mathcal{MA} . While this appears non-intuitive at first, the simultaneous regional encoding of the \mathcal{MA} renders it more powerful than curve-based disambiguation. The symmetry transform sequence depicted here recovers the illusory triangle at one depth and completes the “pacmen” at another (d).

resentation of a vast array of objects in static or dynamic, evolving form, this possibly at all scales.

References

- [1] Sylvain Airault, Oliver Jamet, and Frederic Leymarie. From manual to automatic stereoplotting: Evaluation of different road network capture processes. In *International Archives of Photogrammetry and Remote Sensing*, volume 31, pages 14–18, 1996.
- [2] Jun Aishima, Leo Guibas, Axel Brunger, and Paul Adams. Automated crystallographic building using the medial axis transform of an electron density isosurface. *Acta Crystallographica D — Biological Crystallography*, 61(Part 10):1354–1363, October 2005. <http://journals.iucr.org/d/issues/2005/10/00/gx5065/gx5065bdy.html>.
- [3] Nina Amenta, Marshall Bern, and Manolis Kamvyselis. A new Voronoi-based surface reconstruction algorithm. *Computer Graphics (SIGGRAPH '98)*, pages 415–421, July 1998.
- [4] Nina Amenta, Sunghee Choi, Maria E. Jump, Ravi Krishna Kolluri, and Thomas Wahl. Finding alpha-helices in skeletons. Technical Report TR-02-27, University of Texas at Austin, Computer Science Dept., October 2002.
- [5] Nina Amenta, Sunghee Choi, and Ravi Kolluri. The power crust, unions of balls, and the medial axis transform. *International Journal of Computational Geometry and its Applications*, 19(2-3):127–153, 2001.
- [6] Alexis Angelidis, Pauline Jepp, and Marie-Paule Cani. Implicit modeling with skeleton curves: Controlled blending in contact situations. In *International Conference on Shape Modeling and Applications (SMI'02)*, pages 137–144, Banff, Alberta, Canada, 2002.
- [7] Cecil G. Armstrong, S.J. Bridgett, R.I. Donaghy, R.W. McCune, R.M. McKeag, and D.J. Robinson. Techniques for interactive and automatic idealisation of CAD models. In *Numerical Grid Generation in Computational Field Simulations*, pages 643–662, July 1998.

- [8] Rudolf Arnheim. *Art and Visual Perception: A Psychology of the Creative Eye*. University of California Press, Berkeley, CA, U.S.A., 1974. New version; expanded and revised edition of the 1954 original.
- [9] Dominique Attali and Annick Montanvert. Computing and simplifying 2D and 3D continuous skeletons. *Computer Vision and Image Understanding*, 67(3):261–273, 1997.
- [10] Richard F. W. Bader. *Atoms in Molecules — A Quantum Theory*, volume 22 of *International Series of Monographs on Chemistry*. Clarendon Press, Oxford, UK, 1990. Oxford University Press; Reprint edition (June, 1994).
- [11] Chandrajit Bajaj. Geometric modeling and quantitative visualization of virus ultrastructure. In L. da Fontoura Costa and M. Laublichler, editors, *Modeling Biology: Structures, Behaviors, Evolution*. MIT Press, To appear.
- [12] Chandrajit Bajaj, Zeyun Yu, and Manfred Auer. Volumetric feature extraction and visualization of tomographic molecular imaging. *Journal of Structural Biology*, 144(1–2):132–143, October 2003.
- [13] Yih-En Andrew Ban, Herbert Edelsbrunner, and Johannes Rudolph. Interface surfaces for protein-protein complexes. In *Proceedings of the 8th International Conference on Research in Computational Molecular Biology*, pages 205–212, San Diego, California, USA, March 2004.
- [14] Michael Batty and Sanjay Rana. The automatic definition and generation of axial lines and axial maps. *Environment and Planning B*, 31(4):615–640, 2004.
- [15] Michael Beil, Hans Braxmeier, Frank Fleischer, Volker Schmidt, and Paul Walther. Quantitative analysis of keratin filament networks in scanning electron microscopy images of cancer cells. Submitted for publication, 2005.
- [16] Sylvia Biasotti and Simone Marini. 3D object comparison based on shape descriptors. *International Journal of Computer Applications in Technology*, 23(2/3/4):57–69, 2005.
- [17] Ingmar Bitter, Arie Kaufman, and Mie Sato. Penalized-distance volumetric skeleton algorithm. *IEEE Transactions on Visualization and Computer Graphics*, 7(3):195–206, July–September 2001.

- [18] Rob Blanding, Cole Brooking, Duane Storti, and Mark Ganter. A skeletal-based solid editor. In *Proceedings of the Fifth ACM Symposium on Solid Modeling and Applications*, pages 141–154, Atlanta, GA, May 1999.
- [19] Rob Blanding, George Turkiyyah, Duane Storti, and Mark Ganter. Skeleton-based three-dimensional geometric morphing. *Journal of Computational Geometry: Theory and Applications*, 15(1–3):129–148, February 2000.
- [20] Harry Blum. A transformation for extracting new descriptors of shape. In W. Wathen-Dunn, editor, *Models for the Perception of Speech and Visual Form*, pages 362–380. M.I.T. Press, Cambridge, MA, U.S.A., 1967. Proceedings of a Symposium held in Boston, MA, U.S.A.; November 1964.
- [21] Harry Blum. Biological shape and visual science. *Journal of Theoretical Biology*, 38:205–287, 1973.
- [22] Jean-Daniel Boissonnat, Olivier Devillers, Jacqueline Duquesne, and Mariette Yvinec. Computing Connolly surfaces. *Journal of Molecular Graphics*, 12(1):61–62, 1994.
- [23] Gunilla Borgefors, Ingela Nyström, and Gabriella Sanniti di Baja. Computing skeletons in three dimensions. *Pattern Recognition*, 32(7):1225–1236, July 1999.
- [24] Stewart Brand. Environmental heresies. *TechnologyReview.com*, May 2005.
- [25] Marta Braun. *Picturing Time*. Chicago University Press, IL, USA, 1992.
- [26] J. W. Bruce and Peter J. Giblin. *Curves and Singularities: A Geometrical Introduction to Singularity Theory*. Cambridge University Press, Cambridge, UK, 2nd edition, 1992.
- [27] Jehoshua Bruck, Jie Gao, and Anxiao (Andrew) Jiang. MAP: Medial axis based geometric routing in sensor networks. In *11th Annual International Conference on Mobile Computing and Networking (MobiCom’05)*, pages 88–102, Cologne, Germany, August 2005.
- [28] Ed Burton. Thoughtful drawings: A computational model of the cognitive nature of children’s drawing. In *EUROGRAPHICS’95*, volume 14, pages C–159–C–170, 1995.

- [29] Jason E. Cain, Thibault Nion, Dominique Jeulin, and John F. Bertram. Exogenous BMP-4 amplifies asymmetric ureteric branching in the developing mouse kidney in vitro. *Kidney International*, 67(2):420–431, February 2005.
- [30] Adrijana Car. *Hierarchical Spatial Reasoning: Theoretical Consideration and its Application to Modeling Wayfinding*, volume 10 of *GeoInfo Series*. Department of Geoinformation, Technical University of Vienna, Austria, 1997.
- [31] Arthur Cayley. On contour and slope lines. *The London, Edinburgh and Dublin Philosophical Magazine and Journal of Science*, 18(120):264–268, October 1859.
- [32] Ming-Ching Chang, Frederic F. Leymarie, and Benjamin B. Kimia. 3D shape registration using regularized medial scaffolds. In *Proceedings of the 2nd International Symposium on 3D Data Processing, Visualization and Transmission (3DPVT)*, pages 987–994, Thessaloniki, Greece, September 2004.
- [33] Michael S. Chapman and Michael L. Connolly. *Molecular Surfaces: Calculations, Uses and Representations*, volume F: Crystallography of Biological Macromolecules of *International Tables for Crystallography*, chapter 22.1.2. Kluwer, International Union of Crystallography, Chester, UK, July 2001.
- [34] Ashutosh Chaturvedi and Zhenghong Lee. Three-dimensional segmentation and skeletonization to build an airway tree data structure for small animals. *Physics in Medicine and Biology*, 50(7):1405–1419, April 2005.
- [35] Graham P. Collins. The shapes of space. *Scientific American*, (291):94–103, July 2004.
- [36] Michael L. Connolly. Shape distributions of protein topography. *Biopolymers*, 32(9):1215–1236, 1992.
- [37] David B. Cooper et al. Bayesian virtual pot-assembly from fragments as problems in perceptual-grouping and geometric-learning. In *Proceedings of the International Conference on Pattern Recognition (ICPR'02)*, volume 3, pages 297–302, Quebec City, Canada, August 2002.

- [38] Le Corbusier. *Towards a New Architecture*. Dover, 1985. Translation by Frederick Etchells of "Vers une architecture," first published in French in 1923.
- [39] Joseph J. Crisco, Mohammad A. Upal, and Douglas C. Moore. Advances in quantitative in vivo imaging. *Current Opinions in Orthopedics*, 14(5):351–355, October 2003.
- [40] Luise A. Cullen-McEwen, Gabriel Fricout, Ian S. Harper, Dominique Jeulin, and John F. Bertram. Quantization of 3D ureteric branching morphogenesis in cultured embryonic mouse kidney. *International Journal of Developmental Biology*, 46(8):1049–1055, 2002.
- [41] Silvester Czanner, Roman Ďurikovič, and Hirofumi Inoue. Growth simulation of human embryo brain. In *IEEE 17th Spring Conference on Computer Graphics (SCCG'01)*, pages 139–146, Budmerice, Slovakia, April 2001.
- [42] René Descartes. *Le Monde ou Traité de la lumière*. Claude Clerselier, 1664. Written in 1633; published posthumously in 1664.
- [43] Oliver Deussen, Jörg Hamel, Andreas Raab, Stefan Schlechtweg, and Thomas Strothotte. An illustration technique using hardware-based intersections and skeletons. In *Proceedings of Graphics Interface*, pages 175–182, Kingston, OT, Canada, 1999.
- [44] Oliver Deussen and Thomas Strothotte. Computer-generated pen-and-ink illustration of trees. In *Proc. of the 27th ACM International Conference on Computer Graphics and Interactive Techniques (SIGGRAPH'00)*, pages 13–18, 2000.
- [45] John Dubinski, Luiz N. da Costa, Dalia S. Goldwirth, M. Lecar, and T. Piran. Void evolution and the large-scale structure. *Astrophysical Journal*, 410(2):458–468, 1993.
- [46] Roman Durikovic. Growth simulation of digestive system using function representation and skeleton dynamics. *International Journal on Shape Modeling*, 10(1):31–49, June 2004.
- [47] Roman Durikovic and Silvester Czanner. Growth animation of human organs. *Journal of Visualization and Computer Animation*, 12:287–295, 2001.

- [48] Eric Ferley, Marie-Paul Gascuel, and Dominique Attali. Skeletal reconstruction of branching shapes. *Computer Graphics Forum*, 16(5):283–293, December 1997.
- [49] Pascal Ferraro, Christophe Godin, and Przemyslaw Prusinkiewicz. Toward a quantification of self-similarity in plants. *Fractals*, 13(2):91–109, 2005.
- [50] Paul W. Finn and Lydia E. Kavradi. Computational approaches to drug design. *Algorithmica*, 25:347–371, 1999.
- [51] Stefan Funke. Topological hole detection in wireless sensor networks and its applications. In *Proceedings of the Joint Workshop on Foundations of Mobile Computing*, pages 44–53, Cologne, Germany, September 2005.
- [52] John M. Gauch and Stephen M. Pizer. The intensity axis of symmetry and its application to image segmentation. *IEEE Transactions on Pattern Analysis and Machine Intelligence*, 15(8):753–770, August 1993.
- [53] Roland Geraerts and Mark H. Overmars. Clearance based path optimization for motion planning. In *EEE International Conference on Robotics and Automation (ICRA'04)*, pages 2386–2392, 2004.
- [54] Roland Geraerts and Mark H. Overmars. On improving the clearance for robots in high-dimensional configuration spaces. In *IEEE/RSJ International Conference on Intelligent Robots and Systems (IROS'05)*, pages 4074–4079, 2005.
- [55] Christopher M. Gold. Primal/dual spatial relationships and applications. In *9th International Symposium on Spatial Data Handling (SDH)*, volume 4a, pages 15–27, Beijing, China, August 2000.
- [56] Christopher M. Gold and David Thibault. Map generalization by skeleton retraction. In *Proc. of the 20th International Cartographic Conference (ICC)*, pages 2071–2081, Beijing, China, August 2001. International Cartographic Association.
- [57] Bruce Gooch, Greg Coombe, and Peter Shirley. Artistic vision: Painterly rendering using computer vision techniques. In *Proceedings of the 2nd International Symposium on Non Photorealistic Rendering (NPAR'02)*, pages 83–91, Annecy, France, June 2002.

- [58] Kreshna Gopal, Tod D. Romo, Erick Mckee, Kevin C. Childs, Lalji Kanbi, Reetal Pai, Jacob Smith, James C. Sacchettini, and Thomas R. Ioerger. TEXTAL: Automated crystallographic protein structure determination. In *Proceedings of the Innovative Applications of Artificial Intelligence Conference*, pages 1483–1490, 2005.
- [59] Jonathan Greer. Three-dimensional pattern recognition: An approach to automated interpretation of electron density maps of proteins. *Journal of Molecular Biology*, 82:279–301, 1974.
- [60] Jonathan Greer. Computer skeletonization and automatic electron density map analysis. *Methods in Enzymology*, 115:206–224, November 1985.
- [61] Leonidas J. Guibas, Christopher Holleman, and Lydia E. Kavradi. A probabilistic roadmap planner for flexible objects with a workspace medial axis based sampling approach. In *Proc. Intl. Conf. Intelligent Robots and Systems*, pages 254–260, Kyongju, Korea, 1999. IEEE/RSJ.
- [62] Brower Hatcher, Karl Aspelund, Andrew Willis, Jasper Speicher, David B. Cooper, and Frederic F. Leymarie. Computational schemes for biomimetic sculpture. In *Proceedings of the 5th International Conference on Creativity and Cognition*, pages 22–31, London, U.K., April 2005. ACM.
- [63] Martin Held. *On the computational geometry of pocket machining*. Number 500 in Lecture Notes in Computer Science. Springer-Verlag, Berlin, 1991.
- [64] Martin Held. VRONI: An engineering approach to the reliable and efficient computation of Voronoi diagrams of points and line segments. *Computational Geometry: Theory and Applications*, 18(2):95–123, March 2001.
- [65] Masaki Hilaga, Yoshihisa Shinagawa, Taku Komura, and Toshiyasu L. Kunii. Topology matching for full automatic similarity estimation of 3D shape. In *Proceedings of SIGGRAPH 2001*, Computer Graphics Proceedings, Annual Conference Series, pages 203–212, Los Angeles, CA, USA, August 2001. ACM.
- [66] Bill Hillier. *Space is the Machine — A Configurational Theory of Architecture*. Cambridge University Press, Cambridge, UK, 1996.

- [67] Bill Hillier, Julienne Hanson, and John Peponis. Syntactic analysis of settlements. *Architecture et Comportment/Architecture and Behavior*, 3(3):217–231, 1987.
- [68] Christoph M. Hoffmann. Geometric approaches to mesh generation. In I. Babuska et al., editors, *Modeling, Mesh Generation, and Adaptive Numerical Methods for Partial Differential Equations*, volume 75 of *IMA Volumes in Mathematics and its Applications*, pages 31–52. Springer Verlag, 1995.
- [69] Christopher Holleman and Lydia E. Kavraki. A framework for using the workspace medial axis in PRM planners. In *Proceedings of the International Conference on Robotics and Automation*, pages 1408–1413, San Fransisco, CA, USA, 2000.
- [70] Jun Huan, Deepak Bandyopadhyay, Wei Wang, Jack Snoeyink, Jan Prins, and Alexander Tropsha. Comparing graph representations of protein structure for mining family-specific residue-based packing motifs. *Journal of Computational Biology*, 12(6):657–671, July 2005.
- [71] Vincent Icke and Rien van de Weygaert. Fragmenting the universe. I. Statistics of two-dimensional Voronoi foams. *Astronomy and Astrophysics*, 184:16–32, 1987.
- [72] Vincent Icke and Rien van de Weygaert. The galaxy distribution as a Voronoi foam. *Quarterly Journal of the Royal Astronomical Society*, 32(2):85–112, 1991.
- [73] Takeo Igarashi, Satoshi Matsuoka, and Hidehiko Tanaka. Teddy: A sketching interface for 3D freeform design. In *Proceedings of the 26th annual conference on Computer graphics and interactive techniques (SIGGRAPH'99)*, pages 409–416, 1999.
- [74] Thomas R. Ioerger and Jim C. Sacchettini. Automatic modeling of protein backbones in electron density maps via prediction of C-alpha coordinates. *Acta Crystallographica*, D58(12):2043–2054, 2002.
- [75] Natraj Iyer, Subramaniam Jayanti, Kuiyang Lou, Yagnanarayanan Kalyanaraman, and Karthik Ramani. Three-dimensional shape searching: State-of-the-art review and future trends. *Computer-Aided Design*, 37(5):509–530, April 2005.

-
- [76] Carroll K. Johnson, Michael N. Burnett, and William D. Dunbar. Crystallographic topology and its applications. 1996. <http://www.ornl.gov/sci/ortep/topology.html>.
- [77] Gaetano Kanisza. *Organization in Vision: Essays on Gestalt Perception*. Praeger, 1979.
- [78] Daniel A. Keim, Christian Panse, and Stephen C. North. CartoDraw: A fast algorithm for generating contiguous cartograms. *IEEE Transactions on Visualization and Computer Graphics*, 10(1):95–110, January/February 2004.
- [79] Daniel A. Keim, Christian Panse, and Stephen C. North. Medial-axis-based cartograms. *IEEE Computer Graphics and Applications*, 25(3):60–68, May/June 2005.
- [80] Benjamin B. Kimia. On the role of medial geometry in human vision. *Journal of Physiology*, 97(2–3):155–190, March–May 2003.
- [81] Wolfgang Kohler. *Gestalt Psychology, An Introduction to New Concepts in Modern Psychology*. Liveright Pub. Corp., 1947.
- [82] Jan J. Koenderink and Andrea J. van Doorn. The structure of relief. *Advances in Imaging and Electron Physics*, 103:65–150, 1998.
- [83] Kurt Koffka. *Principles of Gestalt Psychology*. Brace Harcourt, 1935.
- [84] Ilona Kovács, Akos Feher, and Bela Julesz. Medial-point description of shape: A representation for action coding and its psychophysical correlates. *Vision Research*, 38:2323–2333, 1998.
- [85] Ilona Kovács and Bela Julesz. A closed curve is much more than an incomplete one: Effect of closure in figure-ground segmentation. *Proceedings of the National Academy of Science of the USA*, 90(16):7495–7497, August 1993.
- [86] Ilona Kovács and Bela Julesz. Perceptual sensitivity maps within globally defined visual shapes. *Nature*, 370:644–646, 1994.
- [87] Mei-Po Kwan and Jiyeong Lee. Emergency response after 9/11: The potential of real-time 3D GIS for quick emergency response in micro-spatial

- environments. *Computers, Environment and Urban Systems*, 29(2):93–113, 2005.
- [88] Francis Lazarus, Sabine Coquillart, and Pierre Jancene. Axial deformations: An intuitive deformation technique. *Computer-Aided Design*, 26(8):607–613, August 1994.
- [89] Francis Lazarus and Anne Verroust. Level set diagrams of polyhedral objects. In *Proceedings of the Fifth ACM Symposium on Solid Modeling and Applications*, pages 130–140, 1999.
- [90] Jiyeong Lee. 3D data model for representing topological relations of urban features. In *Proceedings of 21st Annual ESRI International User Conference*, San Diego, CA, 2001.
- [91] Jiyeong Lee. A spatial access-oriented implementation of a 3-D GIS topological data model for urban entities. *GeoInformatica*, 8(3):237–264, September 2004.
- [92] Laurence Leherte, Janice Glasgow, Kim Baxter, Evan Steeg, and Suzanne Fortier. Analysis of three-dimensional protein images. *Journal of Artificial Intelligence Research (JAIR)*, 7:125–159, 1997.
- [93] Helena C. G. Leitão and Jorge Stolfi. Information contents of fracture lines. In *8th International Conference in Central Europe on Computer Graphics, Visualization, and Interactive Digital Media*, volume 2, pages 389–395. Univ. of West Bohemia Press, February 2000.
- [94] Robert H. Lewis and Stephen Bridgett. Conic tangency equations and Apollonius problems in biochemistry and pharmacology. *Mathematics and Computers in Simulation*, 61(2):101–114, January 2003.
- [95] Frederic Leymarie. Exploitation of 3D georeferenced datasets in a GIS. In *Proc. International Workshop on HPCN Exploitation of Multimedia Databases*, pages 10–29, Ispra, Italy, March 1997. European Commission, JRC, no. EUR 17349 EN.
- [96] Frederic Leymarie, Nicolas Boichis, Sylvain Airault, and Olivier Jamet. Towards the automation of road extraction processes. In *SPIE European Symposium on Satellite and Remote Sensing III*, volume SPIE-2960, pages 84–95, Taormina, Italy, September 1996.

- [97] Frederic Leymarie, David Cooper, Martha Joukowsky, Benjamin Kimia, David Laidlaw, David Mumford, and Eileen Vote. The SHAPE Lab: New technology and software for archaeologists. In *CAA 2000: Computing Archaeology for Understanding the Past*, volume 931 of *BAR International Series*, pages 79–89, Oxford, UK, April 2001. Archaeopress.
- [98] Frederic Leymarie and Michael Gruber. Applications of virtual reality: Cybermonument & cybercity. In *Proceedings of the 3rd European Digital Cities Conference*, Berlin, Germany, December 1997. European Commission. <http://www.lems.brown.edu/~leymarie/cybercity/>.
- [99] Frederic Leymarie and Martin D. Levine. Simulating the grassfire transform using an active contour model. *IEEE Transactions on Pattern Analysis and Machine Intelligence*, 14(1):56–75, January 1992.
- [100] Frederic Leymarie and Martin D. Levine. Tracking deformable objects in the plane using an active contour model. *IEEE Transactions on Pattern Analysis and Machine Intelligence*, 15(6):617–634, June 1993.
- [101] Frederic F. Leymarie. *Three-Dimensional Shape Representation via Shock Flows*. PhD thesis, Brown University, Providence, RI, USA, May 2003. www.lems.brown.edu/~leymarie/phd/.
- [102] Frederic F. Leymarie and Benjamin B. Kimia. The medial scaffold of 3D unorganized point clouds. Under review, 2006 (expected).
- [103] Frederic F. Leymarie, Benjamin B. Kimia, and Peter J. Giblin. Towards surface regularization via medial axis transitions. In *Proc. of the International Conference on Pattern Recognition (ICPR)*, volume 3, pages 123–126, Cambridge, U.K., August 2004.
- [104] Frederic Fol Leymarie. Aesthetic computing and shape. *Aesthetic Computing*, Paul Fishwick, ed., chapter 14. MIT Press, April 2006.
- [105] Frederic Fol Leymarie and Benjamin B. Kimia. Computation of the shock scaffold for unorganized point clouds in 3D. In *IEEE Proc. of the International Conference on Computer Vision and Pattern Recognition (CVPR)*, volume 1, pages 821–827, 2003.
- [106] Michael Leyton. *Symmetry, Causality, Mind*. MIT press, Cambridge, MA, USA, 1992.

-
- [107] Michael Leyton. *A Generative Theory of Shape*. Number LNCS 2145. Springer-Verlag, 2001.
 - [108] Michael Leyton. The foundations of aesthetics. *Aesthetic Computing*, Paul Fishwick, ed., chapter 13. MIT Press, April 2006.
 - [109] Hongzhi Li. An integrated approach to protein backbone modeling. Master's thesis, Queen's University, Dept. of Computing and Information Science, Kingston, OT, Canada, October 2002.
 - [110] Shuo Liang Lin, Ruth Nussinov, Daniel Fischer, and Haim J. Wolfson. Molecular surface representations by sparse critical points. *Proteins: Structure, Function, and Genetics*, 18:94–101, 1994.
 - [111] Aristid Lindenmayer. Mathematical models for cellular interactions in development: Parts i and ii. *Journal of Theoretical Biology*, 18:280–315, 1968.
 - [112] Paul J. Locher. An empirical investigation of the visual rightness theory of picture perception. *Acta Psychologica*, 114(2):147–164, October 2003.
 - [113] Jean-François Mangin, D. Rivière, A. Cachia, D. Papadopoulos-Orfanos, D. L. Collins, A. C. Evans, and J. Régis. Object-based morphometry of the cerebral cortex. *IEEE Transactions on Medical Imaging*, 23(8):968–982, August 2004.
 - [114] James Clerk Maxwell. On hills and dales. *The London, Edinburgh and Dublin Philosophical Magazine and Journal of Science*, 40(269):421–425, December 1870.
 - [115] Michael McAllister and Jack Snoeyink. Extracting consistent watersheds from digital river and elevation data. In *ASPRS Annual Conference Proceedings — From Image to Information*, Portland, OR, USA, May 1999.
 - [116] Michael McAllister and Jack Snoeyink. Medial axis generalization of river networks. *CaGIS*, 27(2), April 2000. Journal of the Cartography and Geographical Information Society.
 - [117] Fernand Meyer and Petros Maragos. Multiscale morphological segmentations based on watershed, flooding, and eikonal PDE. In M. Nielsen, P. Johansen, O.F. Olsen, and J. Weickert, editors, *Scale-Space Theories*

in Computer Vision, number 1682 in Lecture Notes in Computer Science, pages 351–362. Springer-Verlag, 1999.

- [118] Lee R. Nackman. Two-dimensional critical point configuration graphs. *IEEE Transactions on Pattern Analysis and Machine Intelligence*, 6(4):442–450, July 1984.
- [119] Lee R. Nackman and Stephen M. Pizer. Three-dimensional shape description using the symmetric axis transform i: Theory. *IEEE Transactions on Pattern Analysis and Machine Intelligence*, 7(2):187–202, March 1985.
- [120] Ambjorn Naeve and Jan-Olaf Eklundh. Generalized cylinders - what are they? In C. Arcelli, L.P. Cordella, and G. S. di Baja, editors, *Aspects of Visual Form Processing*, 2nd International Workshop on Visual Form, pages 384–409, Singapore, May-June 1994. IAPR, World Scientific. Workshop held in Capri, Italy.
- [121] M. Näf, Gábor Székely, Ron Kikinis, Martha Elizabeth Shenton, and Olaf Kübler. 3D Voronoi skeletons and their usage for the characterization and recognition of 3D organ shape. *Computer Vision and Image Understanding*, 66(2):147–161, May 1997.
- [122] Ingela Nystrom, Gabriella Sanniti di Baja, and Stina Svensson. Representing volumetric vascular structures using curve skeletons. In *11th International Conference on Image Analysis and Processing (ICIAP'01)*, pages 495–500, Palermo, Italy, September 2001.
- [123] Atsuyuki Okabe, Barry Boots, Kokichi Sugihara, and Sung Nok Chiu. *Spatial Tessellations: Concepts and Applications of Voronoi Diagrams*. Probability and Statistics. Wiley, 2nd edition, 2000.
- [124] Allison M. Okamura. *Haptic Exploration of Unknown Objects*. PhD thesis, Stanford University, Department of Mechanical Engineering, California, USA, June 2000.
- [125] Allison M. Okamura. Uniting haptic exploration and display. In R. A. Jarvis and Al. Zelinsky, editors, *Proc. of the 10th International Symposium on Robotics Research*, volume 6 of *Springer Tracts in Advanced Robotics*, pages 225–238, Lorne, Victoria, Australia, November 2003.

- [126] David S. Paik, Christopher F. Beaulieu, R. Brooke Jeffrey, Geoffrey D. Rubin, and Sandy Napel. Automated flight path planning for virtual endoscopy. *Medical Physics*, 25(5):629–637, May 1998.
- [127] Georgios Papaioannou and Evaggelia-Aggeliki Karabassi. On the automatic assemblage of arbitrary broken solid artefacts. *Image and Vision Computing*, 21(5):401–412, May 2003.
- [128] Georgios Papaioannou, Evaggelia-Aggeliki Karabassi, and Theoharis Theoharis. Reconstruction of three-dimensional objects through matching of their parts. *IEEE Transactions on Pattern Analysis and Machine Intelligence*, 24(1):114–124, January 2002.
- [129] David Parsons and John Canny. Geometric problems in molecular biology and robotics. In R. Altman, D. Brutlag, P. Karp, R. Lathrop, and D. Searls, editors, *Proceedings of the Second International Conference on Intelligent Systems for Molecular Biology (ISMB-94)*, Menlo Park CA, August 1994. AAAI Press.
- [130] Nicholas M. Patrikalakis and Takashi Maekawa. *Shape Interrogation for Computer Aided Design and Manufacturing*. Springer, 2002.
- [131] Alan Penn. Space syntax and spatial cognition — or why the axial line? *Environment and Behavior*, 35(1):30–65, 2003.
- [132] Stephen M. Pizer et al. Deformable M-Reps for 3D medical image segmentation. *International Journal of Computer Vision*, 55(2–3):85–106, 2003.
- [133] Stephen M. Pizer, Kaleem Siddiqi, Gábor Székely, James N. Damon, and Steven W. Zucker. Multiscale medial loci and their properties. *International Journal of Computer Vision*, 55(2–3):155–179, 2003.
- [134] Serge Pontier, Behzad Shariat, and Denis Vandorpe. Weighted skeleton for implicit object reconstruction. In *Proceedings of the 8th ICECGDG*, pages 520–525, Austin, Texas, USA, 1998.
- [135] Liz Potterton, Stuart McNicholas, Eugene Krissinel, Jan Gruber, Kevin Cowtan, Paul Emsley, Garib N. Murshudov, Serge Cohen, Anastassis Perakisd, and Martin Noble. Developments in the CCP4 molecular-graphics project. *Biological Crystallography*, 60(Part 12, Number 1):2288–2294, December 2004. *Acta Crystallographica*, Section D.

- [136] Slava Pranovich. *Structural Sketcher: A Tool for Supporting Architects in Early Stages*. PhD thesis, Computer Science Department, Technische Universiteit Eindhoven, the Netherlands, 2004.
- [137] Slava Pranovich, Henri Achten, Bauke de Vries, and Jack van Wijk. Structural Sketcher: Representing and applying well-structured graphic representations in early design. *International Journal of Architectural Computing*, 3(1):75–92, January 2005.
- [138] M.A. Price and Cecil G. Armstrong. Hexahedral mesh generation by medial surface subdivision: Part I. Solids with convex edges. *International Journal for Numerical Methods in Engineering*, 38(19):3335–3359, October 1995.
- [139] M.A. Price and Cecil G. Armstrong. Hexahedral mesh generation by medial surface subdivision: Part II. Solids with flat and concave edges. *International Journal for Numerical Methods in Engineering*, 40:111–136, January 1997.
- [140] Przemyslaw Prusinkiewicz. Modeling plant growth and development. *Current Opinion in Plant Biology*, 7(1):79–83, 2004.
- [141] Przemyslaw Prusinkiewicz and Aristid Lindenmayer. *The Algorithmic Beauty of Plants*. Springer-Verlag, 1990. <http://algorithmicbotany.org/>.
- [142] Adam Runions, Martin Fuhrer, Brendan Lane, Pavol Federl, Anne-Gaëlle Rolland-Lagan, and Przemyslaw Prusinkiewicz. Modeling and visualization of leaf venation patterns. *ACM Transactions on Graphics*, 24(3):702–711, 2005.
- [143] Thomas B. Sebastian. *Shape-based Object Recognition*. PhD thesis, Brown University, Division of Engineering, Providence, RI, USA, 2001.
- [144] Thomas B. Sebastian, Philip N. Klein, and Benjamin B. Kimia. Recognition of shapes by editing their shock graphs. *IEEE Transactions on Pattern Analysis and Machine Intelligence*, 26(5):550–571, May 2004.
- [145] Thomas B. Sebastian, Hüseyin Tek, Joseph J. Crisco, Scott W. Wolfe, and Benjamin B. Kimia. Segmentation of carpal bones from 3D CT images using skeletally coupled deformable models. *Medical Image Analysis*, 7(1):21–45, March 2003.

- [146] Jean Serra. *Image Analysis and Mathematical Morphology*, volume 1. Academic Press, 1982.
- [147] Damian J. Sheehy, Cecil G. Armstrong, and Desmond J. Robinson. Shape description by medial surface construction. *IEEE Transactions on Visualization and Computer Graphics*, 2(1):62–72, 1996.
- [148] Ilya Shlyakhter, Max Rozenoer, Julie Dorsey, and Seth Teller. Reconstructing 3D tree models from instrumented photographs. *IEEE Computer Graphics and Applications*, 21(3):53–61, May-June 2001.
- [149] Kaleem Siddiqi and Benjamin B. Kimia. A shock grammar for recognition. In *Proceedings of the Conference on Computer Vision and Pattern Recognition (CVPR'96)*, pages 507–513, 1996.
- [150] Kaleem Siddiqi, Benjamin B. Kimia, Allen Tannenbaum, and Steven W. Zucker. Shocks, shapes, and wiggles. *Image and Vision Computing*, 17(5-6):365–373, 1999.
- [151] Kaleem Siddiqi, Ali Shokoufandeh, Sven J. Dickinson, and Steven W. Zucker. Shock graphs and shape matching. *International Journal of Computer Vision*, 35(1):13–32, November 1999.
- [152] Pierre Soille. *Morphological Image Analysis: Principles and Applications*. Springer-Verlag, corr. 2nd printing of the 2nd edition edition, 2004. <http://ams.jrc.it/soille/book2ndprint/>.
- [153] Martin Styner, Guido Gerig, Sarang Joshi, and Stephen Pizer. Automatic and robust computation of 3D medial models incorporating object variability. *International Journal of Computer Vision*, 55(2–3):107–122, November–December 2003.
- [154] Stina Svensson and Gabriella Sanniti di Baja. Simplifying curve skeletons in volume images. *Computer Vision and Image Understanding*, 90(3):242–257, June 2003.
- [155] Gábor Székely. *Shape Characterization by Local Symmetries*. Habilitationsschrift, ETH Zurich, Switzerland, 1996.
- [156] Amir Tamrakar and Benjamin B. Kimia. Medial visual fragments as an intermediate image representation for segmentation and perceptual grouping.

In *Proceedings of IEEE Workshop on Perceptual Organization in Computer Vision, POCV*, page 47, 2004.

- [157] Marek Teichmann and Seth Teller. Assisted articulation of closed polygonal models. In *Proc. 9th Eurographics Workshop on Animation and Simulation*, Lisbon, Portugal, August 31 - September 1 1998.
- [158] Huseyin Tek and Benjamin B. Kimia. Boundary smoothing via symmetry transforms. *Journal of Mathematical Imaging and Vision*, 14(3):211–223, May 2001.
- [159] Huseyin Tek and Benjamin B. Kimia. Symmetry maps of free-form curve segments via wave propagation. *International Journal of Computer Vision*, 54(1-3):35–81, August 2003. Kluwer Academic.
- [160] David Thibault and Christopher M. Gold. Terrain reconstruction from contours by skeleton generation. *GeoInformatica*, 4(4):349–373, December 2000.
- [161] David Charles Thompson. *Feasibility of a Skeletal Modeler for Conceptual Mechanical Design*. PhD thesis, University of Texas at Austin, December 2000.
- [162] Richard E. Toth. Theory and language in landscape analysis, planning, and evaluation. *Landscape Ecology*, 1(4):193–201, 1988.
- [163] Patrick Tresset and Frederic Fol Leymarie. Generative portrait sketching. In Hal Thwaites, editor, *Proceedings of the 11th International Conference on Virtual Systems and Multimedia (VSMM)*, pages 739–748, Ghent, Belgium, October 2005. <http://belgium.vsmm.org/>.
- [164] Alasdair Turner, Alan Penn, and Bill Hillier. An algorithmic definition of the axial map. *Environment and Planning B: Planning and Design*, 32(3):425–444, 2005.
- [165] Gokturk Ucoluk and Ismail Hakki Toroslu. Automatic reconstruction of broken 3-D surface. *Computers and Graphics*, 23(4):573–582, August 1999.
- [166] Cornelius W.A.M. van Overveld and Brian Wyvill. Polygon inflation for animated models: A method for the extrusion of arbitrary polygon meshes.

Journal of Visualization and Computer Animation, 8(1):3–16, January–March 1997.

- [167] Gert J. van Tonder. Order and complexity of naturalistic landscapes: On creation, depiction and perception of Japanese dry rock gardens. 2006 (in Press). <http://www.ipc.kit.ac.jp/gert/publications/publications.html>.
- [168] Gert J. van Tonder. Recovery of visual structure in illustrated Japanese gardens. 2006 (in Press). <http://www.ipc.kit.ac.jp/gert/publications/publications.html>.
- [169] Gert J. van Tonder and Yoshimichi Ejima. From image segmentation to anti-textons. *Perception*, 29(10):1231–1247, October 2000.
- [170] Gert J. van Tonder and Yoshimichi Ejima. The patchwork engine: Image segmentation from image symmetries. *Neural Networks*, 13(3):291–303, April 2000.
- [171] Gert J. van Tonder and Yoshimichi Ejima. Flexible computation of shape symmetries within the maximal disk paradigm. *IEEE Transactions on Systems, Man, and Cybernetics, Part B*, 33(3):535–540, June 2003.
- [172] Gert J. van Tonder and Michael J. Lyons. Visual perception in Japanese rock garden design. *Axiomathes*, 15(3):353–371, September 2005.
- [173] Gert J. van Tonder, Michael J. Lyons, and Yoshimichi Ejima. Visual structure of a Japanese Zen garden. *Nature*, (419):359–360, September 2002.
- [174] Anne Verroust and Francis Lazarus. Extracting skeletal curves from 3D scattered data. *The Visual Computer*, 16(1):15–25, 2000.
- [175] Luc Vincent and Pierre Soille. Watersheds in digital spaces: An efficient algorithm based on immersion simulations. *IEEE Transactions on Pattern Analysis and Machine Intelligence*, 13(6):583–598, June 1991.
- [176] Lawson Wade and Richard E. Parent. Automated generation of control skeletons for use in animation. *The Visual Computer*, 18(2):97–110, 2002.
- [177] Ming Wan, Frank Dachele, and Arie Kaufman. Distance-field based skeletons for virtual navigation. In *Proceedings of the conference on Visualization '01*, pages 239–246, San Diego, CA, USA, October 2001.

- [178] Ron Wein, Jur P. van den Berg, and Dan Halperin. The visibility-Voronoi complex and its applications. In *Proc. 21st ACM Symposium on Computational Geometry*, pages 63–72, Pisa, Italy, June 2005.
- [179] Steffen Werner and Paul Long. Cognition meets Le Corbusier — Cognitive principles of architectural design. In C. Freksa et al., editors, *Spatial Cognition III*, volume 2685 of *Lecture Notes in Computer Science*, pages 112–126. 2003.
- [180] Max Wertheimer. Laws of organization in perceptual forms. In W. D. Ellis, editor, *A Source Book of Gestalt Psychology*. Brace Harcourt (1938), 1923.
- [181] Geoffrey B. West, James H. Brown, and Brian J. Enquist. A general model for the structure and allometry of plant vascular systems. *Nature*, 400:664–667, August 1999.
- [182] Rien van de Weygaert. The cosmic foam: Stochastic geometry and spatial clustering across the universe. In E.D. Feigelson and G.J. Babu, editors, *Statistical Challenges in Modern Astronomy III*, pages 175–196. Springer-Verlag (in 2003), 2001.
- [183] Rien van de Weygaert and Vincent Icke. Fragmenting the universe. II. Voronoi vertices as Abell clusters. *Astronomy and Astrophysics*, 213(1–2):1–9, April 1989.
- [184] M. Wienstroerer and H. Mathieu. Reverse process simulation for forging using the medial axis transformation. In *Advanced Technology of Plasticity*, volume 2, pages 973–978, 2002. Proc. of the 7th ICTP, Oct. 2002, Yokohama, Japan.
- [185] Andrew Willis. *Stochastic 3D Geometric Models for Classification, Deformation, and Estimation*. PhD thesis, Division of Engineering, Brown University, Providence, RI, USA, May 2004.
- [186] Andrew Willis and David B. Cooper. Alignment of multiple non-overlapping axially symmetric 3D datasets. In *Proceedings of ICPR*, volume 4, pages 96–99, Cambridge, UK, August 2004.
- [187] Andrew Willis and David B. Cooper. Bayesian assembly of 3D axially symmetric shapes from fragments. In *Proceedings of CVPR*, volume 1, pages 82–89, June 2004.

- [188] Steven A. Wilmarth, Nancy M. Amato, and Peter F. Stiller. Motion planning for a rigid body using random networks on the medial axis of the free space. In *Proc. of the 15th Annual Symposium of Computational Geometry*, pages 173–180, Miami, FL, June 1999. ACM.
- [189] Franz-Erich Wolter and K.-I. Friese. Local and global geometric methods for analysis interrogation, reconstruction, modification and design of shape. In *Proceedings of Computer Graphics International (CGI'00)*, pages 137–151, Geneva, Switzerland, June 2000. IEEE Computer Society.
- [190] Franz-Erich Wolter, Niklas Peinecke, and Martin Reuter. *Geometric Modeling of Complex Shapes and Engineering Artifacts*, volume 1 of *Encyclopedia of Computational Mechanics*, chapter 16. Wiley, 2004.
- [191] Robert C. Zeleznik, Kenneth P. Herndon, and John F. Hughes. SKETCH: An interface for sketching 3D scenes. In *Computer Graphics Proceedings, SIGGRAPH'96*, Annual Conference Series, pages 163–170, New Orleans, Louisiana, USA, August 1996. ACM.
- [192] Yong Zhou, Arie Kaufman, and Arthur W. Toga. Three-dimensional skeleton and centerline generation based on an approximate minimum distance field. *The Visual Computer*, 14(7):303–314, 1998.